AGU ADVANCING EARTH AND SPACE SCIENCES

AGU Advances

RESEARCH ARTICLE
10.1029/2024AV001175

Permafrost Formation in a Meandering River Floodplain

Madison M. Douglas[1,2], Gen K. Li[1,3], A. Joshua West[4], Yutian Ke[1], Joel C. Rowland[5], Nathan Brown[6], Jon Schwenk[5], Preston C. Kemeny[1,7], Anastasia Piliouras[5,8], Woodward W. Fischer[1], and Michael P. Lamb[1]

[1]Division of Geological and Planetary Sciences, California Institute of Technology, Pasadena, CA, USA, [2]Department of Earth and Planetary Sciences, Massachusetts Institute of Technology, Cambridge, MA, USA, [3]Department of Earth Science, University of California Santa Barbara, Santa Barbara, CA, USA, [4]Department of Earth Sciences, University of Southern California, Los Angeles, CA, USA, [5]Los Alamos National Laboratory, Los Alamos, NM, USA, [6]Department of Earth and Environmental Sciences, University of Texas at Arlington, Arlington, TX, USA, [7]Department of the Geophysical Sciences, University of Chicago, Chicago, IL, USA, [8]Department of Geosciences, University of Pennsylvania, University Park, PA, USA

Abstract Permafrost influences 25% of land in the Northern Hemisphere, where it stabilizes the ground beneath communities and infrastructure and sequesters carbon. However, the coevolution of permafrost, river dynamics, and vegetation in Arctic environments remains poorly understood. As rivers meander, they erode the floodplain at cutbanks and build new land through bar deposition, creating sequences of landforms with distinct formation ages. Here we mapped these sequences along the Koyukuk River floodplain, Alaska, analyzing permafrost occurrence, and landform and vegetation types. We used radiocarbon and optically stimulated luminescence (OSL) dating to develop a floodplain age map. Deposit ages ranged from modern to 10 ka, with more younger deposits near the modern channel. Permafrost rapidly reached 50% areal extent in all deposits older than 200 years then gradually increased up to ~85% extent for deposits greater than 4 Kyr old. Permafrost extent correlated with increases in black spruce and wetland abundance, as well as increases in permafrost extent within wetland, and shrub and scrub vegetation classes. We developed an inverse model to constrain permafrost formation rate as a function of air temperature. Permafrost extent initially increased by ~25% per century, in pace with vegetation succession, before decelerating to <10% per millennia as insulating overbank mud and moss slowly accumulated. Modern permafrost extent on the Koyukuk floodplain therefore reflects a dynamic balance between widespread, time-varying permafrost formation and rapid, localized degradation due to cutbank erosion that might trigger a rapid loss of permafrost with climatic warming.

Plain Language Summary Arctic rivers rework their floodplains, eroding permafrost from one riverbank while depositing unfrozen sediment on the opposite bank, where permafrost may eventually form. While permafrost is often considered a stable reservoir for carbon or platform for construction, permafrost extent in river floodplains is continually changing. To better understand the fate of permafrost in a warming world, we mapped and dated floodplain deposits, determined permafrost extent, and characterized vegetation types along the Koyukuk River in Alaska. Permafrost was present in floodplain deposits of all ages but was most abundant in older areas of the floodplain, where thick mosses and muddy flood deposits insulated the ground from warm summer air temperatures. Younger areas of the floodplain initially had patchy permafrost but rapidly formed permafrost in 50% of their area within 200 years. Permafrost formation then slowed and reached a maximum extent about 85% of deposit area after 4,000 years. We propose that early, rapid permafrost generation is driven by vegetation growth and succession while the later, slow rate of permafrost generation is determined by the rates at which muddy flood deposits and moss accumulate, providing insulation to the ground. Under a warming climate, our modeling shows that permafrost generation in new river deposits will be even slower or cease entirely, making river floodplains susceptible to rapid loss of permafrost via river erosion.

Peer Review The peer review history for this article is available as a PDF in the Supporting Information.

Key Points:

- River meandering resets permafrost development and vegetation succession by eroding old floodplain areas and depositing new land
- On the Koyukuk River, permafrost rapidly forms in new deposits, but it takes over 4 Kyr to develop to its full areal extent of 85%
- The rate of permafrost formation is likely linked to vegetation succession on younger and overbank deposition on older floodplain areas

Supporting Information:

Supporting Information may be found in the online version of this article.

Correspondence to:

M. M. Douglas,
mmdouglas@berkeley.edu

Citation:

Douglas, M. M., Li, G. K., West, A. J., Ke, Y., Rowland, J. C., Brown, N., et al. (2024). Permafrost formation in a meandering river floodplain. *AGU Advances*, *5*, e2024AV001175. https://doi.org/10.1029/2024AV001175

Received 16 JAN 2024
Accepted 13 JUN 2024

Author Contributions:

Conceptualization: Madison M. Douglas, A. Joshua West, Joel C. Rowland, Woodward W. Fischer, Michael P. Lamb
Formal analysis: Madison M. Douglas
Funding acquisition: Joel C. Rowland, Woodward W. Fischer, Michael P. Lamb
Investigation: Madison M. Douglas, Gen K. Li, A. Joshua West, Yutian Ke, Joel C. Rowland, Nathan Brown, Jon Schwenk, Preston C. Kemeny, Anastasia Piliouras, Michael P. Lamb
Methodology: Gen K. Li, A. Joshua West, Yutian Ke, Joel C. Rowland,

1. Introduction

Much of the Northern Hemisphere is underlain by permafrost—ground that has remained below 0°C for at least two consecutive years—but its age and material properties vary widely (French & Shur, 2010; Obu et al., 2019; van Everdingen, 2005). Permafrost is vulnerable to collapse and erosion upon thaw, so understanding the extent of frozen ground is critical for hazard prediction and mitigation in the Arctic (Karjalainen et al., 2019). In addition, permafrost in sedimentary deposits and soils is especially rich in organic carbon (OC); the thaw and

Nathan Brown, Preston C. Kemeny, Michael P. Lamb
Project administration: A. Joshua West
Supervision: Michael P. Lamb
Writing – original draft: Madison M. Douglas
Writing – review & editing: Gen K. Li, A. Joshua West, Yutian Ke, Joel C. Rowland, Nathan Brown, Jon Schwenk, Preston C. Kemeny, Anastasia Piliouras, Woodward W. Fischer, Michael P. Lamb

mobilization of this sediment might result in oxidation of OC and generate a positive feedback on the warming climate (Schwab et al., 2020; Turetsky et al., 2020; Wild et al., 2019). Thus, the fate of permafrost is linked to global climate change (Chadburn et al., 2017; Smith et al., 2022).

Permafrost loss is typically thought to occur from the top down; that is, warmer mean annual temperatures allow the seasonal thaw layer (active layer) to penetrate deeper into the permafrost (Biskaborn et al., 2019; Isaksen et al., 2016). In this view, the ground nearest to the land surface (e.g., in the top meter) is most vulnerable to thaw. However, in river corridors the dynamics of permafrost development and thaw play out much deeper due to channel dynamics (Roux et al., 2017; Stephani et al., 2020). Rivers such as the Yukon can meander or laterally migrate at several meters per year (Rowland, Crosby, et al., 2023; Rowland, Schwenk, et al., 2023), eroding older floodplain deposits that typically contain discontinuous permafrost (Douglas et al., 2022; Mann et al., 1995). The river can thaw permafrost far below the thickness of the active layer to the depth of the river or deeper (Crampton, 1979; Minsley et al., 2012). In a warming climate, there is concern that the rates of riverbank erosion will accelerate (Costard et al., 2003; Douglas et al., 2023). Thus, in addition to top-down thaw, river corridors are susceptible to rapid loss of deep permafrost due to bank erosion.

However, the loss of deep permafrost by bank erosion can be partially or completely offset by permafrost generation in new river deposits. Rivers tend to maintain a constant channel width, such that erosion on the cutbank side is in approximate balance with bar deposition on the opposite riverbank (Leopold & Wolman, 1957; Parker et al., 2011). If permafrost can rapidly form in new bar deposits, it could offset permafrost loss from bank erosion, resulting in a stable areal permafrost extent despite bank erosion. Alternatively, if permafrost formation is slow compared to permafrost loss from bank erosion, there would be a net decline in permafrost extent as a result of river meandering. Thus, determining the rate of permafrost formation in river deposits is essential to predict the fate of permafrost in river floodplains. While substantial progress has been made in understanding riverbank erosion in permafrost (e.g., Douglas et al., 2023; Gautier et al., 2021; Kanevskiy et al., 2016), comparatively less is known about the rates and mechanisms of permafrost formation in new river deposits, which is our focus here.

Meandering rivers preferentially rework deposits near the active channel, generating a decline in the fraction of deposits preserved as a function of their age, with older deposits located further from the modern river (Bradley & Tucker, 2013; Lauer & Willenbring, 2010; Torres et al., 2017). These differences in deposit ages across the floodplain can be used to understand permafrost formation in time. Discontinuous permafrost formation on North American floodplains is typically described in concert with vegetation succession. Pioneer willows (*Salix alaxensis*) first colonize new point bars, giving way to poplars (*Populus balsamifera*) within 10–15 years and then white spruce (*Picea glauca*) becoming dominant within 200 years (Drury, 1956; Yarie et al., 1998). At this point, moss (*Sphagnum*) can grow, since deciduous trees no longer cover the forest floor with leaves; the moss provides insulation and significantly reduces ground temperatures (Viereck, 1970). Permafrost growth prevents groundwater infiltration, gradually increasing the surface water content and creating conditions favorable for further moss and black spruce (*Picea mariana*) growth (Drury, 1956; Jorgenson et al., 1998). Eventually, the active layer is too saturated for white spruce to grow and the oldest floodplain deposits transition to organic-rich peat bogs with sparse black spruce with high permafrost extent (Kreig & Reger, 1982; Shur & Jorgenson, 2007).

In addition to vegetation succession, landform type, deposit grain size, and proximity to the river might influence permafrost formation as deposits age. Point bars tend to be coarse-grained (e.g., sand or gravel), have thicknesses that scale with the river depth, and are thawed when initially formed. While near the river, bar deposits remain thawed at depth owing to heat provided by the river water, forming a talik (Crampton, 1979; Minsley et al., 2012). As the river migrates away from the deposit, heat is lost from the deposit to the atmosphere, allowing epigenetic permafrost formation from the base of the active layer downwards (Gill, 1975; Kreig & Reger, 1982). Overbank floods bring fine sediment that builds the floodplain on top of the bar deposits and form sandy levees, which produce a sequence of scroll ridges with muddy swales in between when these deposits are abandoned (Miall, 2006). This is important because finer sediment tends to have a lower thermal diffusivity and higher water retention and therefore may promote permafrost formation (Shur & Jorgenson, 2007). In addition to changes in grainsize, ground elevation could play a role in permafrost formation. Abandoned levees are comparatively high ground, and floodplain elevation tends to increase in time due to overbank accretion (Lauer & Parker, 2008). On one hand, both high elevations and greater distance from river decrease the likelihood of inundation by warm flood water that can cause rapid ground thaw (Zheng et al., 2019). On the other hand, these floods provide the

Figure 1. Field photos of the Koyukuk River, Alaska. (a) Map of Alaska with the Yukon River system shown in light blue and the Koyukuk River in dark blue. (b) Aerial image showing scroll bar complexes outlined by vegetation across the Koyukuk River floodplain near Huslia, Alaska. Boat for scale (white circle) is the same boat depicted in (d). (c) Seasonally frozen bank with large white spruce and willow trees tipping into the river as the bank erodes. (d) Cutbank containing permafrost and ice wedges overlain by a thick layer of peat and mosses with few trees.

overbank mud that insulates and builds the floodplain, and therefore may ultimately promote permafrost formation in the long run (Jorgenson et al., 1998; Stephani et al., 2020).

While the early stages of vegetation succession on river bars and the initiation of permafrost formation are known to happen in ∼200 years (Viereck, 1970), it is unclear whether this newly formed permafrost is patchy or extensive. Beyond 200 years, the areal extent of permafrost and its rate of formation are poorly constrained. These older deposits are particularly important because these have the greatest permafrost extents and contain ice- and organic-rich strata that are vulnerable to ground collapse and carbon release upon thaw. White spruce forest can persist on floodplains for at least 500 years (Mann et al., 1995), implying that later stages of permafrost formation might occur gradually. Radiocarbon dating of basal peat layers in the oldest deposits in the Colville Delta of Alaska ranged from 3 to 4 Kyr (Jorgenson et al., 1998), but these ages provide a lower bound on the timescale required to reach a maximum permafrost extent since they indicate the time since moss began to accumulate rather than the time since sediment was deposited. Radiocarbon dating of wood deposited in sandy bar indicated that locations currently occupied by black spruce and peat in the Tanana floodplain were occupied by the river over 3,000 BP (Mann et al., 1995). These studies suggest that permafrost begins forming in newly deposited floodplain within centuries, but it could take thousands of years for permafrost to reach its full areal extent.

Here we built on this previous work by measuring permafrost extent, vegetation type, and landforms in the discontinuous permafrost floodplain of the Koyukuk River, located in central Alaska. Our goal was to quantify permafrost extents and rates of permafrost generation, and to evaluate whether those extents and rates were affected by floodplain landform type, vegetation type, and deposit age. We took advantage of the sequences of scroll bars formed by former paths of the meandering river to map floodplain chronosequences, and we used radiocarbon and optically stimulated luminescence (OSL) to quantify ages. We used permafrost probe measurements and remote sensing products to measure permafrost extent, and landform and vegetation types. Finally, we formulated an inverse problem to constrain potential permafrost growth and degradation histories over time with a simplified numerical model and ran it to match permafrost extent at present day, taking advantage of the shared climatic conditions experienced across the floodplain.

2. Field Site: Koyukuk River, Alaska

The Koyukuk River flows south from its headwaters in the Brooks Range through lowlands containing discontinuous permafrost to join the Yukon River (Figure 1a). The Koyukuk contributes 12% of the mean annual water and sediment discharge and makes up 11% of the catchment area of the Yukon River as measured at Pilot Station (Brabets et al., 2000). We conducted field work on a 30 km long reach of the river near the village of Huslia, Alaska in June to early July of 2018, and in May and late September in 2022. From 1981 to 2010, Huslia had a mean annual air temperature of −3.6°C and mean annual precipitation of 31 cm/year (Daly et al., 2018). The ground temperature in the well-drained eolian deposits beneath the town was 1.8°C at 3.7 m depth below the surface (Laxton & Coates, 2010) and the ground temperature in an exposed permafrost riverbank was −0.4°C at 2.4 m depth below the surface (Rowland, Crosby, et al., 2023; Rowland, Schwenk, et al., 2023). The edges of the

10.1029/2024AV001175

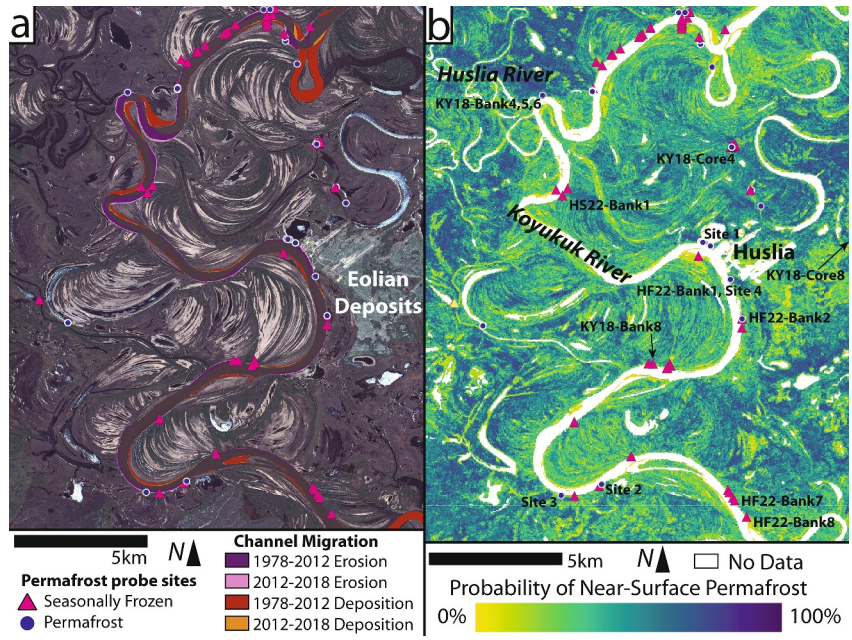

Figure 2. Permafrost occurrence and bank erosion along the Koyukuk River. (a) Floodplain sampling locations from summer 2018 field campaign near the village of Huslia, Alaska. Channel migration masks show areas of erosion and deposition calculated using SCREAM (Rowland et al., 2016) based on 1978–2012 and 2012–2018 Alaska High-Altitude Photography and Worldview imagery (Rowland & Stauffer, 2019). Basemap satellite imagery ©Maxar 2018. (b) Pastick et al. (2015) 30 m-resolution near-surface (within upper 1 m of soil column) permafrost probability map for the Koyukuk River floodplain. Radiocarbon and OSL sample sites from this study are labeled. No Data values shown in white include rivers, lakes, and infrastructure within the town of Huslia.

Koyukuk floodplain are defined by eolian deposits from sand dunes that covered the region during the last ice age, predecessors to the present-day Nogahabara dunes, that ceased being active 15,350–25,850 cal BP (Farquharson et al., 2011). Climate reconstructions indicate that the region experienced an interval of colder air temperatures from ~13 to 11.5 ka during the Younger Dryas, then air temperatures stabilized at modern values at ~8 ka (Alley, 2004; Meyer et al., 2010). Today, the Koyukuk River primarily reworks sediment from its own fluvial deposits.

The Koyukuk River transits the floodplain near Huslia as a single-threaded, meandering channel (Figure 2a). The much smaller Huslia River is the only tributary to the Koyukuk within our 80 km river length study reach, and we assumed the Koyukuk has a similar water discharge, sediment supply, and grain size throughout this river reach. Borehole data indicates that permafrost in the Koyukuk floodplain is up to 31 m thick (Jorgenson et al., 2008). The Koyukuk rarely experiences ice jams (White & Eames, 1999), but portions of the floodplain are frequently inundated (Pekel et al., 2016), most likely due to sheet flooding when the river exceeds bankfull stage or preferential routing of flow through secondary channels.

Vegetation in the Koyukuk floodplain is closely tied to surface morphology. Trees commonly grow on the ridges of scroll bars, contrasting with grasses filling frequently inundated scroll swales, making scroll bars visible in drone and remote sensing imagery (Figure 1b). Floodplain areas with near-surface permafrost tend to contain sparse white spruce, black spruce, and thick layers of moss and peat at the ground surface as well as thermokarst lakes (Nowacki et al., 2003). Riverbanks containing permafrost are frequently overhung, where peat slumps down over thermoerosional niches thawed back at the water line (Figure 1d). In contrast, floodplain regions without permafrost contain willows, poplars, white spruce, and sparse black spruce (Figure 1c). In these respects, the Koyukuk shares similar features with other well-studied floodplains in central Alaska, including the Kuskokwin (e.g., Drury, 1956) and Tanana (e.g., Viereck, 1970) Rivers.

3. Methods

To understand the interplay between permafrost, vegetation, and geomorphology in the Koyukuk floodplain, we measured permafrost presence and extent (Section 3.1) and dated deposit age using radiocarbon and OSL

(Section 3.2). Based on field observations and remote sensing data sets, we mapped the relative age, geomorphology, vegetation, and permafrost areal extent of floodplain deposits (Section 3.3). We then combined the relative age map with the radiocarbon and OSL dating results to determine the age of deposits across the floodplain (Section 3.4). Using the deposit age and permafrost extent, we developed a simplified inversion model for permafrost areal extent through time as a function of air temperature (Section 3.5).

3.1. Permafrost Measurements

Measurements of the seasonal thaw depth in the floodplain were obtained using a 1-m (in summer 2018) or 2-m (in fall 2022) long permafrost probe. With practice, it was possible to distinguish permafrost from other obstructions, such as tree roots, cohesive mud, and pebbles. In this study, we defined permafrost operationally as frozen sediment with sufficient pore or ground ice to resist probing, consistent with ground control data sets for large-scale permafrost mapping (Pastick et al., 2015). All other locations are described as seasonally frozen. In total, we made 141 vertical and 146 horizontal (into the side of eroding riverbanks) permafrost probe measurements, which were validated against visual observations of pore and ground ice in locations where we dug pits or took cores for sampling (Section 3.2). The 141 vertical measurements include two permafrost depth surveys (n = 14, 16) taken in 2018 with a 1-m probe in a random walk to characterize local variability in active layer thickness.

3.2. Field Sampling and Analysis

Field samples were taken across a range of erosional and depositional environments on the floodplain (Figures 2a and 2c). Methods are summarized here with details in Texts S1 and S2 of the Supporting Information S1, and some results from these analyses were previously reported (Douglas et al., 2021, 2022).

We collected samples of wood, peat, and plant material for radiocarbon analysis to infer deposit ages, prioritizing sticks that were imbricated (deposited parallel to bedding or bedforms). We used hand trowels to sample riverbanks and shallow bars, a hand auger for deep unfrozen sediment, and a snow, ice and permafrost research establishment (SIPRE) corer for permafrost. Samples were kept cool in the field and transported frozen back to Caltech, where they were stored at −15°C. Samples were then rinsed with MiliQ water and stored in combusted glass vials before being shipped to the National Ocean Sciences Accelerator Mass Spectrometry (NOSAMS) facility in Woods Hole (fall 2018 samples) or UC Irvine (UCI) (spring 2022 (HS22) and fall 2022 (HF22) samples) for radiocarbon dating. Results were reported as fraction modern (Fm) and uncalibrated radiocarbon years (BP) with uncertainties reported as ±1SD (Table S1 in Supporting Information S1). We then used CALIBomb (R. W. Reimer & Reimer, 2023) to convert from Fm to calibrated ages (cal BP, defined as years before 1950). We used the Intcal20 curve for pre-bomb samples and the unsmoothed Northern Hemisphere Zone 1 curve for post-bomb samples (P. J. Reimer et al., 2004, 2020) and reported the most probable midpoint age with 1SD variation (Table S2 in Supporting Information S1) (del Valle et al., 2014).

Optically stimulated luminescence (OSL) samples were collected to measure the burial duration of floodplain sediment. To collect these samples, we used a mallet to pound in opaque PVC pipe to sandy bank sediment under an opaque tarp to avoid exposure to sunlight. Quartz grains were analyzed using OSL and K-feldspar grains were analyzed using post-infrared infrared stimulated luminescence (IRSL). Both measurements agreed within error, though the K-feldspar grains had slightly lower ages, possibly indicating incomplete bleaching. Detailed analytical procedures and results for these samples are described in Text S2 of the Supporting Information S1, and subsequent analyses and interpretations used only quartz OSL data.

3.3. Mapping and Remote Sensing

We compared field measurements of permafrost occurrence and active layer thickness with a previously published map of near-surface permafrost probability produced using decision and regression tree modeling (Figure 2b) (Pastick et al., 2015). The map training data set contained over 17,000 permafrost probe measurements, though none within our study site, and cross-validation tests indicated 85% accuracy (Pastick et al., 2015). We classified each field measurement site as having or not having permafrost, combining multiple measurements per stratigraphic column or map pixel. We then selected a threshold probability to distinguish permafrost and non-permafrost from the intersection of the true positives and true negatives curves of our field measurements (Figure 4a).

We used satellite imagery to map floodplain deposit relative age in QGIS 3.4. We inferred relative age from cross-cutting scroll bar complexes, since one scroll bar truncated by a second scroll bar must be older than the second, truncating deposit. We selected the youngest possible age class for each depositional surface that maintained mapping internal consistency. Relative age relationships are inferred in some cases (e.g., across the Koyukuk River) because scroll bar truncation surfaces are not observed. In addition, gaps between scroll bar complexes are present where the Huslia River enters the main channel of the Koyukuk and eolian deposits are eroded by the river (Figure 2a). Thus, there could be differences in the depositional age of scroll bars mapped to have the same relative age.

Based on field observations of correlations between vegetation and floodplain landforms, we used the shape and extent of optically identifiable vegetation types in satellite imagery to map floodplain geomorphic units. Mapping was done manually on Maxar imagery (2 m, ©2018), Landsat imagery (30 m), and the National Land Cover Dataset (Wickham et al., 2021). The landscape was classified into the following units: eolian deposits, the town of Huslia, floodplain ridges, floodplain swales, lakes (both thermokarst and oxbow lakes) and secondary channels, overbank deposits (levee and channel splay deposits from the Koyukuk River and secondary floodplain channels), unvegetated bars, Huslia River deposits, and undifferentiated floodplain (river deposits that lack distinct scroll bars). We cross-checked our geomorphic unit mapping against the 2016 National Landcover Dataset (NLCD) produced by spectral classification of Landsat imagery (30 m) combined with ecological surveys (Wickham et al., 2021). We mapped the surficial extent of geomorphic units but did not attempt to estimate their thickness.

Using the relative age and geomorphic maps, we inferred previous locations of the Koyukuk River. Oxbow lakes must have been connected by channels that did not cut across older floodplain deposits due to the law of superposition. The dimensions of oxbow lakes also imply that the Koyukuk River has maintained a roughly similar width and sinuosity through time. In some cases, we were able to infer prior connections between recent (young relative age) oxbow lakes that appear consistent with the modern channel bend wavelength and curvature, and we included these connecting segments in our map.

3.4. Floodplain Deposit Ages

We used radiocarbon and OSL measurements from across the floodplain to calibrate a relation between deposit relative and absolute age (see Texts S1 and S2 in Supporting Information S1). To produce this relation, we excluded 4 of 36 radiocarbon measurements and 1 of 8 OSL measurements because they were inconsistent with scroll bar cross-cutting relations or other radiocarbon or OSL measurements in the same stratigraphic column. Potential outliers for each relative age bin were not excluded because we expect some variability due to gaps between cross-cutting scrolls. The excluded OSL sample, KY18-Bank4-OSL-260 cm, was removed since it was 6.4 Kyr older than an OSL and 7.1 Kyr older than radiocarbon samples taken at the same sampling site, indicating that this sediment was incompletely bleached during its last transport event. Excluded radiocarbon samples consisted of very young (<200 years cal BP) KY18 radiocarbon samples from <1 m depth when these contradicted dates from the same or cross-cutting deposits, since these shallow samples were likely within the active layer. We also excluded 2 HF22 samples taken from the same relatively young point bar, which had very low OC content (<1 wt%) and very old ages (~1 and 14 kBP). These samples likely contained a mix of organics with sediment containing radiocarbon-dead petrogenic OC and therefore do not reflect the age of the deposit. For stratigraphic columns with multiple measurements of woody debris ^{14}C content that were similar (within hundreds of years), we selected the youngest age as most representative of the time of deposition and burial. Using the remaining samples, we used a moving mean fit with a trailing 2 relative age bin window of deposit age versus relative age and reported uncertainty as the 25%–75% range for samples within each window. This fit was used to assign absolute ages to each floodplain deposit in the relative age map. Although no radiocarbon or OSL samples were taken with a relative age of 8, we estimated its corresponding absolute age using the same trailing moving mean window spanning relative ages 7 and 8.

3.5. Permafrost Formation and Degradation Model

To constrain the rates of permafrost formation and degradation following bar formation, we developed a simplified numerical model to evaluate scenarios that could reproduce modern permafrost extents. To estimate permafrost formation rates, we posed the spatial extent of permafrost as an inverse problem based on the data for deposit age and permafrost content. Since the floodplain deposits are located next to each other, we assumed that

they have experienced the same climatic history and should have the same function for permafrost formation and degradation through time. We expected that the rate of vegetation succession and other floodplain processes that alter permafrost extent (e.g., silt deposition by overbank floods) are spatially uniform and depend on deposit age. To model the fraction of the deposit area with permafrost (ψ_{pf}, dimensionless fraction between 0 and 1), we defined a permafrost growth function G (fraction of floodplain area/yr) as:

$$G \equiv \frac{d\psi_{pf}}{dt}. \tag{1}$$

We assumed a functional form for G such that the permafrost growth rate increases linearly with colder air temperatures (T_{air}; °C) (e.g., Delisle, 1998), and decreases with deposit age (t; years):

$$G = -\frac{C_1 T_{air}}{t/t_0 + 1}, \tag{2}$$

in where C_1 (fraction of floodplain area/°C/yr) and timescale t_0 (years) are empirical constants. We propose Equation 2 for the cases where $T_{air} < 0$°C (i.e., $G > 0$). For the case of constant air temperature, integrating Equations 1 and 2 yields

$$\psi_{pf}(t) = -C_1 t_0 T_{air} \ln\left(\frac{t}{t_0} + 1\right) + C_2, \tag{3}$$

where the integration constant $C_2 = 0$ using the boundary condition of $\psi_{pf} = 0$ at $t = 0$ years. The logarithmic form of Equation 3 is justified based on our forthcoming observations (Section 4.4) of rapid initial formation of permafrost in the first 200 years and slower subsequent formation.

Numerous factors—the amplitude of annual air temperature variations, deposit grain size, vegetation cover, and snow cover—are known to affect permafrost occurrence and active layer thickness (Anisimov et al., 1997). However, our main purpose was to evaluate possible trajectories of permafrost formation and degradation over centuries to millennia, and we consider mean annual air temperature to provide a first-order control (Obu et al., 2019). We evaluated Equation 2 using T_{air} estimates obtained from a compilation of pollen temperature anomaly estimates across North America and Europe and observed temperature anomalies for recent decades (Marsicek et al., 2018), which was linearly interpolated for model runs then shifted so that the temperatures at present reproduce mean values from 1981 to 2010 (−3.6°C at Huslia) (Daly et al., 2018). This temperature record shows similar trends to local records of temperature anomalies obtained from midges and lake cores in interior Alaska (Kaufman et al., 2016) and includes the dramatic increase of air temperatures in recent decades due to polar amplification of climate change (England et al., 2021).

We calculated ψ_{pf} from the time of the oldest floodplain deposits onwards using Equations 1 and 2 in a forward model. We used Euler's method, so that at timestep $i + 1$, the permafrost extent for a given deposit was:

$$\psi_{pf,i+1} = \psi_{pf,i} + G dt \tag{4}$$

where $dt = 1$ year and $\psi_{pf} = 0$ at $t = 0$ years. We used absolute deposit ages and tracked permafrost formation and degradation at each timestep for portions of the floodplain that had been deposited. To determine best-fit parameters for C_1 and t_0 we ran the model iteratively using Matlab nonlinear optimizer fmincon.m to find values with the highest R^2 with the fractional area of each deposit age containing permafrost in the present day. Using these best-fit values, we ran the model to evaluate the most likely history for permafrost formation and degradation in the Koyukuk floodplain.

4. Results

4.1. Permafrost Field Measurements

Permafrost probe surveys revealed significant local variability in active layer thickness (Figure 3). The measurements ($n = 35$) near Core 4 converged to a bimodal distribution of active layer depth, with one mode at 65 cm

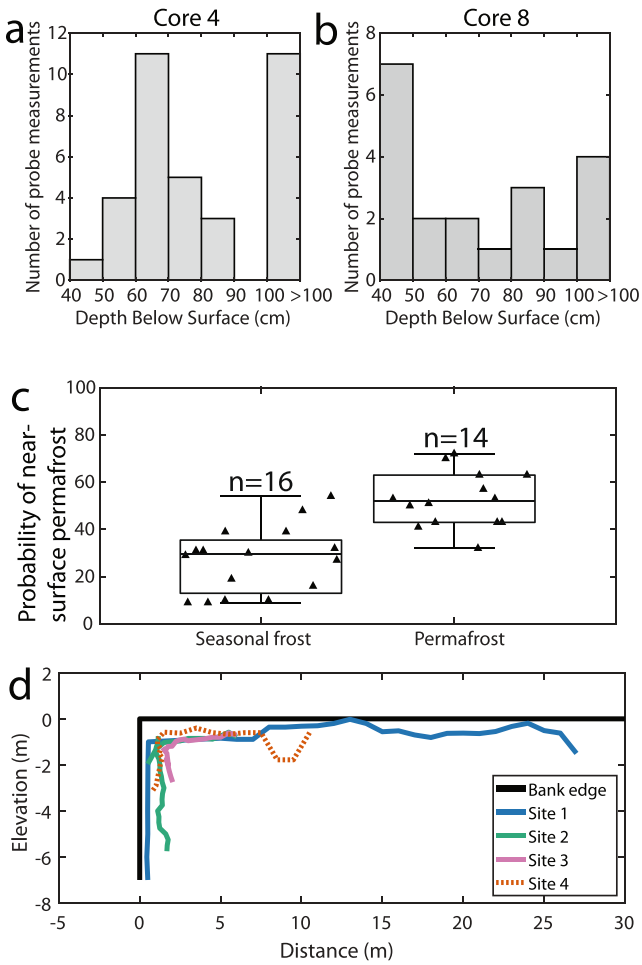

Figure 3. Field observations of permafrost occurrence, with site locations shown in Figure 2b. (a and b) Histograms of permafrost depth surveys measured using a 1-m permafrost probe near (a) Core 4 (1 July 2018) and (b) Core 8 (6 July 2018). Measurements of >100 cm were recorded when the 1-m probe could be pushed flush with the ground surface. (c) Box & whisker plot of probability of permafrost for 1-m probe sites from Pastick et al. (2015) mapping, grouped by whether we observed permafrost or not. (d) Permafrost occurrence (measured with 2-m probe) plotted as depth below the top of river cutbanks versus distance along the top of the eroding cutbank at four different locations in September 2022. The edge of the bank is plotted as a black line, and the location of permafrost within each bank as colored lines, with the distance between the black and colored lines showing the thickness of the thawed layer along the eroding bank face or from the top of the floodplain downwards.

depth and another mode for locations where permafrost may have been at depths greater than 1 m or absent altogether (Figure 3a). The depths measured near Core 8 also did not generate a centralized unimodal distribution (Figure 3b), though fewer measurements were made at this site (n = 18 vs. n = 35). Measurements from both sites showed a minimum thaw depth of ~40 cm and a tail of the distribution extending beyond 1 m depth.

We compared our field observations to the modeled probability of near-surface permafrost by Pastick et al. (2015) at each sampling location. Our probe surveys found near-surface permafrost in 69% and 78% of measurements at the Core 4 and Core 8 sites, respectively (Figure 3b), in comparison to predicted probabilities of 72% and 50% for the 1–2 pixels (pixel size = 30 m) that contained each survey (Pastick et al., 2015). Overall, sites that lacked permafrost but were seasonally frozen (n = 16) exhibited a much lower modeled probability of near-surface permafrost than sites with permafrost (n = 14; Figure 3c). The 25th–75th percentiles of the distributions of probabilities for frozen and unfrozen did not overlap, which supported using the published permafrost map to extrapolate our field measurements across floodplain deposits.

In addition to comparing the spatial distribution of permafrost at single locations, we measured thaw layer thickness in transects along the face and top of eroding cutbanks in fall 2022 (Figure 3d). We found that the bank had thawed back horizontally at least 40 cm from its face at all four sites and this sediment was thawed but not eroded. The floodplain active layer (measured top-down) became steadily thinner over 5–10 m distance back from the edge of the bank. Beyond that distance, the active layer thickness varied more with the rise and fall of scroll ridges (visible at Site 1) and was no longer monotonically decreasing (as at Site 3).

4.2. Permafrost Mapping

We used field observations of permafrost occurrence and found that a 40% probability cutoff for the probability map from Pastick et al. (2015) produced a reasonable map of floodplain permafrost extent (Figure 2). Since Pastick et al. (2015) generated their map using remote sensing products predating our field work, some of our sampling locations were mapped as open water or barren ground and were assumed to lack permafrost ("NoData" in Figure 2b). Overall, the map misclassified a total of 10 non-permafrost sites and 8 permafrost sites out of 84, giving 79% accuracy. Most misclassified sites had active layer thicknesses greater than 1 m, likely because the training data set included mostly 1-m permafrost probe measurements (Pastick et al., 2015). Other misclassifications were due to the 30-m spatial resolution of the data set, since fine-scale topographic variability from overbank deposits and channel levees accounted for 4 misclassifications. Finally, Pastick et al. (2015) misclassified permafrost locations next to water bodies, including 3 on a sandy riverbank next to the Koyukuk and 1 permafrost site misclassified as a floodplain lake. Therefore, using a 40% probability threshold for the Pastick et al. (2015) allowed us to classify locations with active layer thicknesses greater than 1 m and minimized misclassifications.

4.3. Floodplain Geomorphology

We observed abundant scroll bars that revealed the spatial and temporal pattern of the Koyukuk River and its secondary channels re-surfacing the floodplain (Figure 5). The relative age map shows the spatial distribution of scroll bars, with 8 generations of deposits visible (Figure 5a). In general, older deposits and older channel cutoffs were preserved farther from the modern river channel (Figure 5a). Abundant lakes and secondary channels

10.1029/2024AV001175

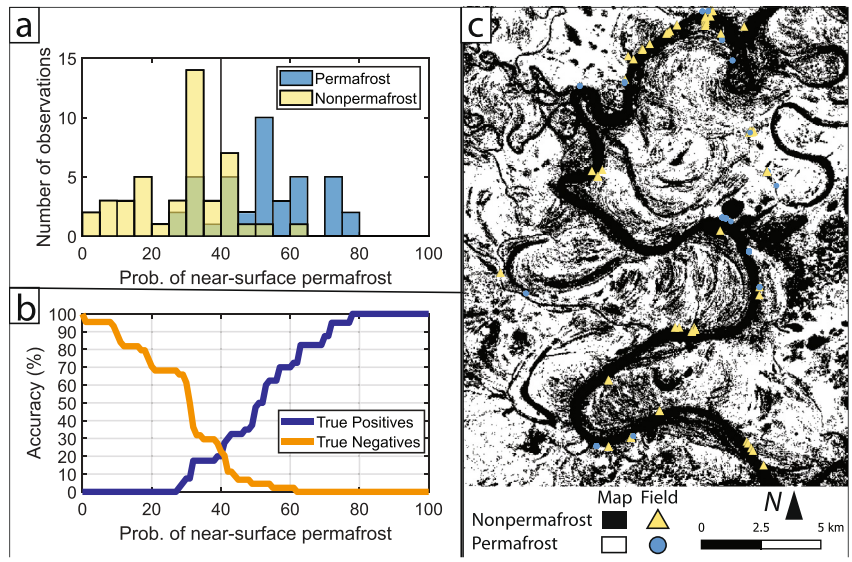

Figure 4. Comparison of permafrost field observations with Pastick et al. (2015) map of permafrost probability. (a) Observations of permafrost using 1- and 2-m permafrost probe measurements, floodplain cores, and observations and lateral permafrost probing on exposed cutbanks plotted versus the mapped probability of permafrost in each location. (b) The number of true positives and true negatives in field data for selected probability thresholds. (c) Map of the probability of permafrost in the top 1 m of the soil column for the Koyukuk River floodplain near Huslia, AK (Pastick et al., 2015). Areas shaded white contain near-surface permafrost (≥40% probability) and areas shaded in black do not contain near-surface permafrost (<40% probability), overlain with field observations of permafrost (blue circles) and non-permafrost (yellow triangles) displayed in (a).

connected the main river to distant parts of the floodplain. Some secondary channels had meandered, generating their own scroll bars, while others located in oxbow lakes and grassy swales were sinuous but showed little evidence of lateral migration (Figure 5c).

In addition, we observed consistent differences in the behavior and types of geomorphic units generated by Koyukuk River bends with low versus high curvature (Figure 5b). High-curvature bends, such as where the Huslia River enters the Koyukuk, rapidly translated downstream and primarily eroded into the deposits of previous translating bends (Figure 5b). These left a record of frequent cutoffs, with oxbows linked by secondary channels that extend perpendicularly to the meander translating downstream (Figure 5c). Translating meanders primarily generated evergreen or wetland forests without clear vegetation alternation or scroll ridges and troughs, and these were bisected by overbank deposits extending from secondary channels. In contrast, expanding bends, such as the one eroding into the village of Huslia, migrated more slowly and generated well-ordered alternating forested ridges with intervening grassy swales (Figure 5c). These deposits contained some internal discontinuities that likely originated from changes in the direction of maximum meandering which eroded a portion of the point bar (Figure 5a).

The geomorphic units making up the Koyukuk floodplain changed with the relative age of the deposits (Figure 5c). Forested scrolls comprised the majority of new floodplain deposits, and their proportion of floodplain area decreased roughly linearly with relative age (Figure 5c). Younger forested scroll deposits contained evergreen forest (Figure 5d), and we interpreted that the raised elevation of scroll ridges prevents flooding and allows white spruce forests to establish. Grassy swales (generally formed by expanding meanders) were moderately abundant on young deposits and then decreased for older deposits. These corresponded roughly to the mixed forest classification on younger deposits and herbaceous wetlands on older deposits in the NLCD map (Figure 5d). The swales of younger scroll bars contained grasses and deciduous trees, and swales in older deposits transitioned to mixed forest and then herbaceous wetlands. Translating meanders made up a slightly lower proportion of the scroll bar area than expanding meanders in young floodplain deposits (Figure 6a). However, translating meanders were preferentially erased on older areas of the floodplain. Selective erosion and/or burial of deposits from translating bends accounted for the decrease in forested scroll and increase in overbank deposit fractional area while other geomorphic units had a relatively constant fractional area for young floodplain deposits (Figure 6b).

10.1029/2024AV001175

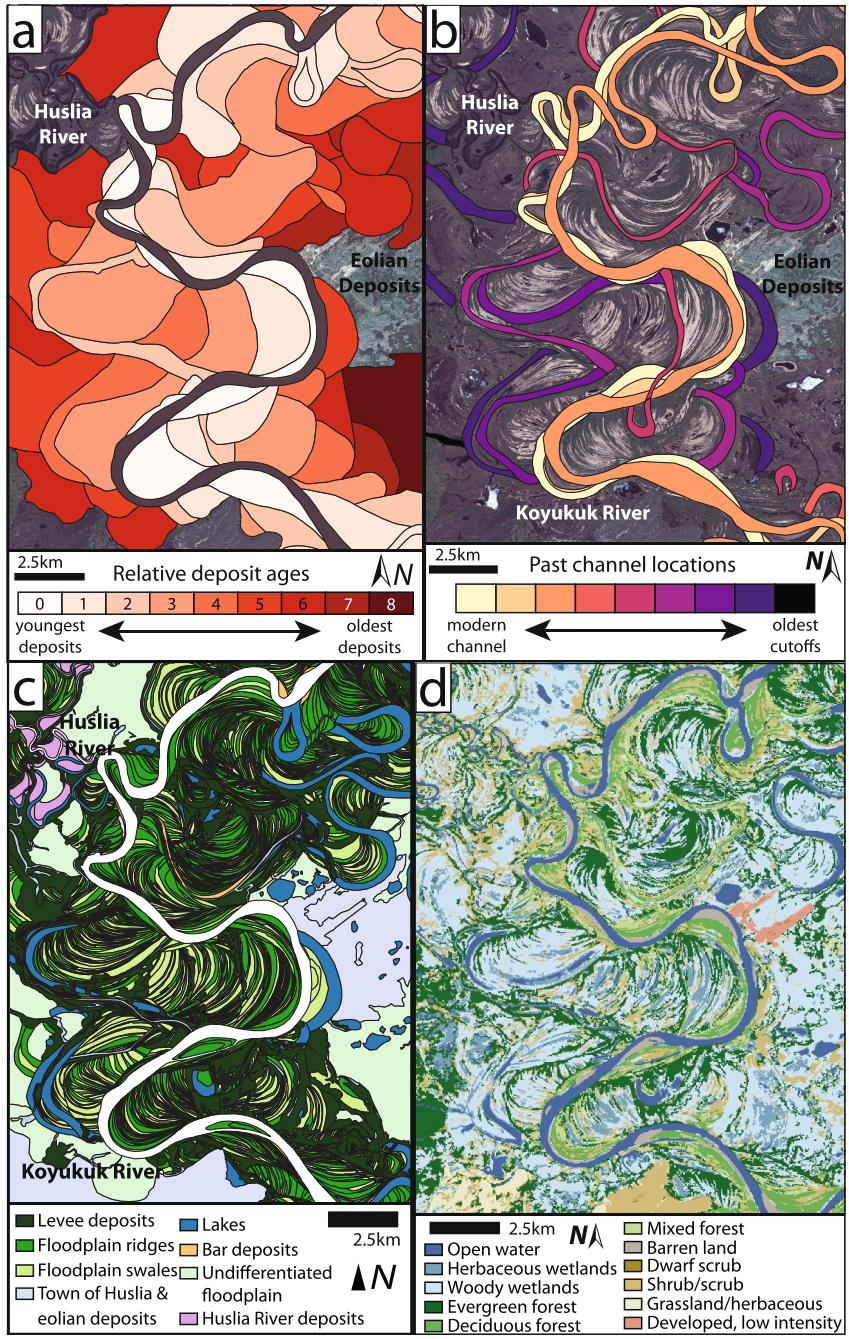

Figure 5. Hand-drawn geomorphic map of the Koyukuk River floodplain from satellite imagery. (a) Map of the relative age of floodplain deposits produced from cross-cutting relationships of scroll bars. (b) Inferred (and undated) previous locations of the Koyukuk River with satellite imagery basemap ©Maxar 2018. (c) Geomorphic map of Koyukuk River floodplain surrounding the village of Huslia, Alaska. (d) National Land Cover Dataset for the floodplain near Huslia, Alaska.

The fraction of overbank deposits peaked at moderate relative floodplain ages, while the area of undifferentiated floodplain unit dominated older floodplain deposits (Figure 6b). This undifferentiated unit, in which clear scroll bar sequences had been mostly erased but evidence of lateral migration remained, corresponded to forested and herbaceous wetlands in the NLCD and high probabilities of near-surface permafrost (Figure 6c). Overbank deposits and moss growth likely gradually buried and decreased the area occupied by distinct scroll bars. The area of floodplain covered by lakes remained roughly constant with deposit relative age (Figure 6b). Lakes comprised approximately 10% of the floodplain for all relative ages, though younger deposits contained oxbow lakes while

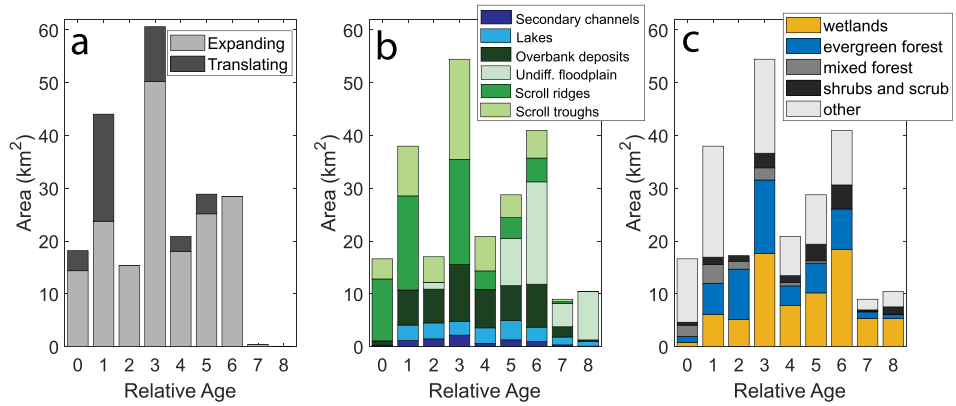

Figure 6. Floodplain properties versus ranked relative deposit age. Plots of the area of (a) translating versus expanding bends, (b) geomorphic units, and (c) NLCD vegetation classification.

older deposits contained rounder thermokarst lakes. We observed oxbows being filled in over time by overbank deposits and static secondary channels but did not observe secondary channels in thermokarst lakes.

4.4. Permafrost Occurrence in the Floodplain Through Time

The combination of OSL and radiocarbon ages indicated that Koyukuk floodplain deposits post-date the Last Glacial Maximum (~20 ka). In total, woody debris ages from 2018 to 2022 ranged from modern to 13.6 cal Kyr BP (Tables S1 and S2 in Supporting Information S1). OSL results, which directly date the time since exposure to sunlight of floodplain sands, gave ages up to 11.7 ± 1.7 Kyr (see Tables S3 and S4 in Supporting Information S1). Floodplain deposits closer to the modern channel tended to have younger ages, and most of the area of the floodplain was below 4 ka (Figure 7a). The oldest floodplain deposits, greater than 6 Kyr old, were a small, distal fraction of the floodplain area but contained woody debris and OSL ages three times the median age of floodplain deposits. Therefore, the Koyukuk River reworked all sampled locations and the majority of its floodplain since 14 ka, producing a wide distribution of ages with significantly older deposits located far from the modern river.

We compared patterns in floodplain geomorphology and permafrost occurrence versus floodplain deposit age calculated from radiocarbon and OSL measurements (Figure 7a; Table S5 in Supporting Information S1). Permafrost was most abundant on older deposits further from the modern channel (Figures 7b and 7c) though it was still present on younger areas of the floodplain. Deposits that were hundreds of years old (1st and 2nd relative age deposits) had patchy near-surface permafrost underlying less than 30% of the ground surface. The age of floodplain deposits did not increase linearly with relative age, and instead there were multiple generations of very young deposits and long gaps between older deposition ages (Figure 7b). The youngest floodplain deposits contained sporadic permafrost (Figure 7c), excluding the possibility that permafrost formed syngenetically as sediment aggraded on point bars. In contrast, older deposits had a much higher fraction of area containing near-surface permafrost. We observed ice-rich permafrost in deposits dated to ~4 ka or older. Permafrost extent was patchy on deposits <0.18 ka and became prevalent for deposits >1 ka. The oldest deposits, which date to 10 Kyr, had ubiquitous permafrost and thermokarst features.

Most floodplain deposits were relatively young, with more than 50% of the floodplain consisting of bars deposited less than 3 ka (Figure 8a). Approximately 20% of the floodplain had been reworked in the last 700 years, while less than 10% of floodplain area consists of deposits from 5 to 10 ka. There was significant uncertainty in the fraction of deposits aged 2–4 ka, which comprised approximately 70% of floodplain area (Figure 8a). Overall, the river appeared to rework younger deposits rapidly while simultaneously preserving a small area of very old deposits (Bradley & Tucker, 2013; Ielpi, Viero, et al., 2023; Torres et al., 2017). However, our results showed a jump in floodplain preservation between deposits less than 200 years old and moderately aged deposits. This was not observed in prior work but might indicate that permafrost rivers are more likely to revisit younger deposits (which typically contain less permafrost) versus older deposits when compared to meandering rivers without permafrost.

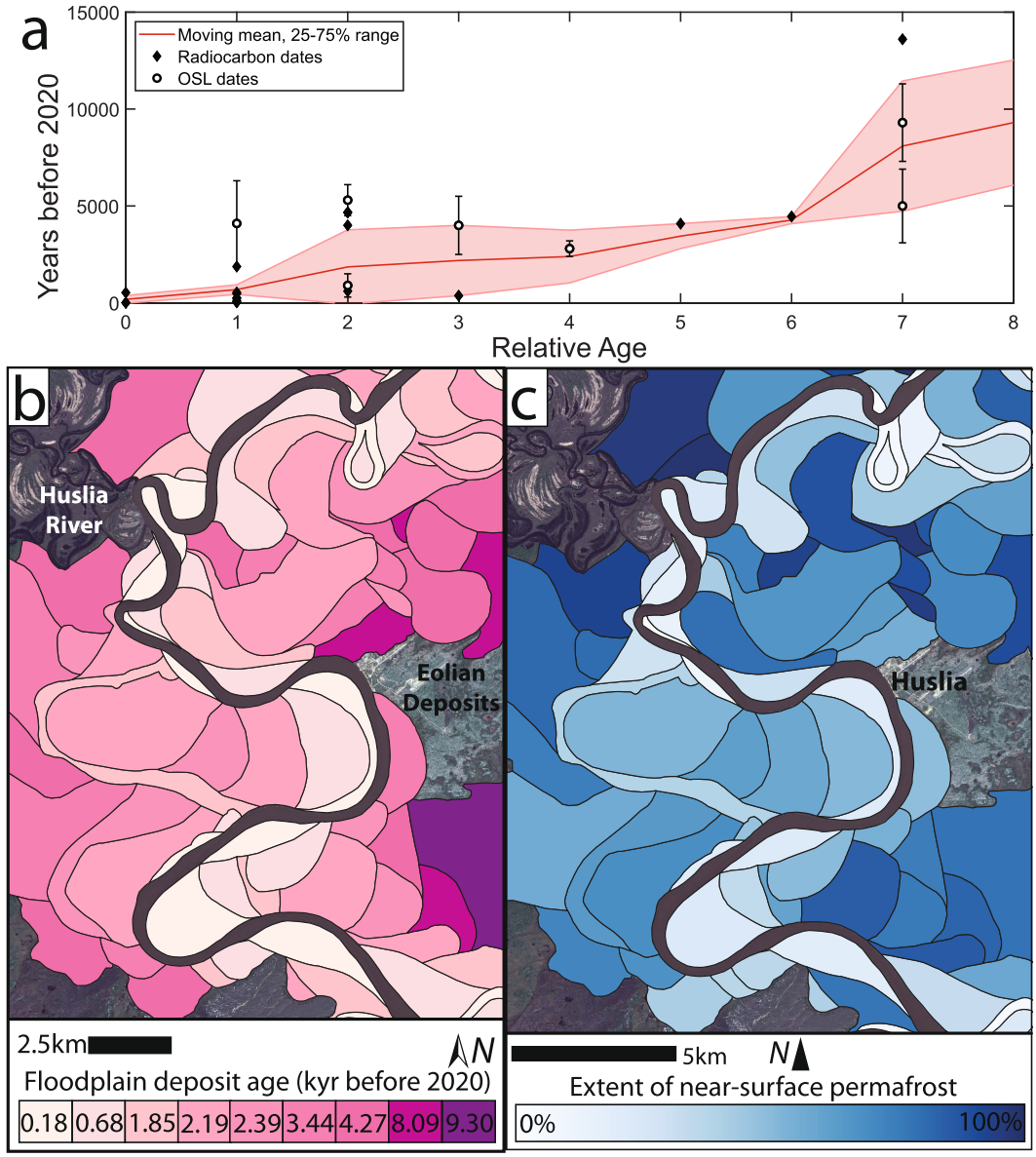

Figure 7. (a) Radiocarbon and OSL ages fit to deposit relative age (0 is youngest, 8 is the oldest) to develop an absolute age calibration for floodplain deposits shown as a moving median with 25%–75% range envelopes in red. Maps of (b) inferred absolute deposit age and (c) fraction of each floodplain deposit containing permafrost for the Koyukuk River floodplain near Huslia, AK (Pastick et al., 2015). Each deposit is color-coded by the fraction of ground that contains near-surface permafrost (≥40% probability in a given pixel).

To compare permafrost formation and forest succession, we determined the fraction of land classified as evergreen forest, mixed or deciduous forest, wetlands, and shrubs and scrub that contained permafrost for each deposit age (Figure 8b). This NCLD classification does not correspond directly with the successional communities in this setting—specifically, the evergreen forest classification includes locations observed in the field to have both black and white spruce. The shrubs and scrub class corresponded to pioneering willows as well as wetland vegetation that may have included stunted black spruce trees. Acknowledging this uncertainty, we found that increased permafrost extent coincided with changes in vegetation type as well as increases in permafrost extent within each vegetation type. Prior to 3.4 ka, much of the floodplain is covered by evergreen forest, with lower proportions of mixed forest, wetlands, and shrubs and scrub. Following 4 ka, there was sparse mixed forest and ~30% of the floodplain was occupied by evergreens, wetlands, and shrubs and scrub (Figure 8b). Except for coniferous forests, all vegetation types experienced gradually increasing permafrost extent through 4 ka,

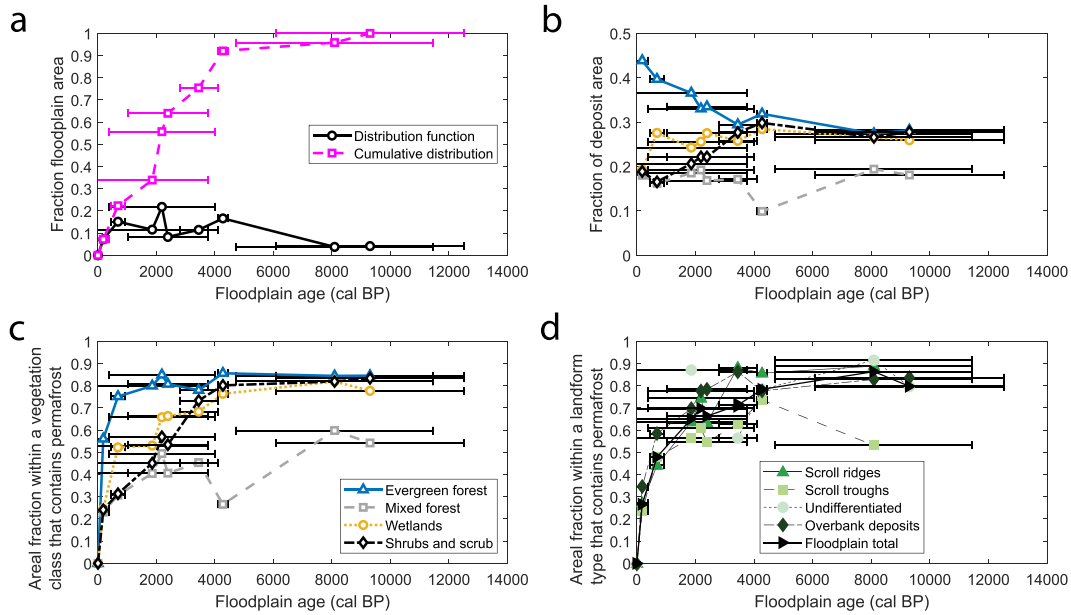

Figure 8. Floodplain permafrost, vegetation, and deposit preservation as a function of time since deposits were formed. (a) The fraction of floodplain area occupied by deposits of each age (black line) and the cumulative distribution of deposit ages (pink dashed line). (b) The fraction of floodplain containing vegetation classes from the National Land Cover Dataset. We plot four main vegetation classes: evergreen forest, deciduous and mixed forest, woody and herbaceous wetlands, and shrubs and scrub (including dwarf scrub, scrub/shrub, grassland/herbaceous). Legend in panel (c). (c) The fraction of floodplain area for each vegetation class that contains permafrost plotted versus deposit age. (d) The fraction of floodplain area for each geomorphic unit that consists of permafrost plotted versus deposit age. Horizontal error bars encompass 25%–75% age distribution.

regardless of NLCD classification (Figure 8c). All vegetation types in deposits older than 4 ka had the same permafrost extent, except for mixed and deciduous forests, which contained notably less permafrost (Figure 8c). These results are consistent with prior work that found vegetation succession to an evergreen forest with discontinuous permafrost taking place over approximately 200 years, though this progression was not resolved in detail due to most of the floodplain being much older than 200 years (e.g., Jorgenson et al., 1998; Viereck, 1970; see Section 1). Instead, our results indicate that a steady increase in permafrost extent within wetlands and shrub/scrub accompanied the replacement of permafrost-poor mixed and deciduous forest with evergreen forests, gradually producing more continuous permafrost on a 4 Kyr timescale.

Permafrost extent across all geomorphic units increased rapidly for the first ~200 years before increasing more slowly to values of 85% (Figure 8d). Total permafrost extent (black line in Figure 8d) was ~25% for the youngest floodplain deposits, increased rapidly to approximately 50% for deposits 680 years old, then increased linearly and at a slower pace up to ~85% for deposits greater than 4 Kyr old. The initial increase ($G \sim 50\%$ of deposit area/680 years) in permafrost extent corresponds to vegetation succession-driven permafrost formation, while other floodplain processes must drive the subsequent gradual increase in permafrost extent from ~700 to 4,000 years ($G \sim 35\%$ of deposit area/3,300 years). While deposit age had the strongest correlation with permafrost extent, there were slight variations in permafrost extent with deposit geomorphology with overbank flood deposits and undifferentiated floodplain having a higher permafrost extent for similar age deposits. For a given deposit age, scroll ridges had a greater permafrost extent than scroll troughs, and neither geomorphic unit was visible in the oldest floodplain deposits potentially due to burial by moss growth and fine overbank sediment (Figure 8d). These oldest deposits contained primarily permafrost-rich undifferentiated units vegetated by evergreens, wetlands, and shrub/scrub and correspond to black spruce bogs. Together, spatial patterns of permafrost, vegetation, and geomorphology imply that rapid, early permafrost formation is primarily driven by vegetation, while later, slower permafrost formation rates are set by the formation rate of undifferentiated floodplain units, which can be approximated by deposit age.

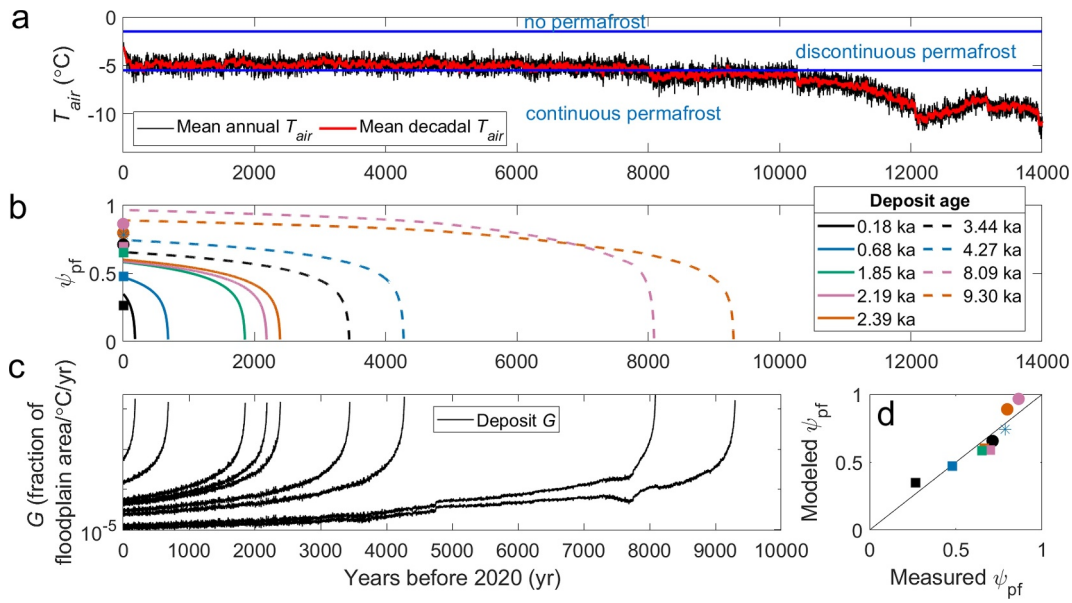

Figure 9. (a) Estimated mean annual air temperatures with 1SD shaded uncertainty for Huslia, AK based on values from Marsicek et al. (2018). Horizontal blue lines denote temperature ranges for continuous, discontinuous, and no permafrost for alluvial deposits from Jorgenson et al. (2008). (b) The fraction of sedimentary deposits of different ages that are predicted to be underlain by permafrost through time. Model results for deposits of different ages are shown as solid or dashed lines, and points on *y* axis are modern fraction permafrost from mapping. (c) The model-predicted rate of permafrost growth (*G*; fraction of deposit area/yr) through time. (d) Modeled versus measured permafrost extent for each deposit age, with $R^2 = 0.81$. The symbols and coloring for each point are the same as in panel (b).

4.5. Permafrost Model Results

To understand the temporal evolution of floodplain permafrost extent during this second period of slower permafrost formation, we used model runs to evaluate the history of permafrost growth and degradation through the present day (see Section 3.5). We used observations of floodplain deposit ages and permafrost occurrence to frame an inverse problem to determine when and how rapidly permafrost had formed through time as a function of mean annual air temperature. This model differs from previous efforts (e.g., Anisimov et al., 1997) because it accounts for the spatial and temporal heterogeneity in permafrost growth rather than looking at a single vertical section. Thus, it provides insight into early permafrost formation due to vegetation succession as well as the distinctive changes in vegetation and floodplain hydrology that occur thousands of years after sediment is deposited.

The Koyukuk floodplain near Huslia has experienced gradual warming over thousands of years and a recent, rapid increase in air temperature (Marsicek et al., 2018). Mean annual air temperatures were much colder, approximately −10°C, prior to 10 ka (Figure 9a). Then, temperatures warmed to −7°C until 8 ka before rising to approximately −5°C until warming in recent decades. Comparing the air temperature record with the modern extent of permafrost in fluvial deposits (Jorgenson et al., 2008) indicates that the Koyukuk likely had continuous permafrost in its floodplain until 10 ka when air temperatures rose and the floodplain likely transitioned to discontinuous permafrost (Figure 9a).

Fitting the permafrost growth model to deposit age and permafrost extent for the Koyukuk River floodplain produced best-fit parameters of $C_1 = 2.1 \times 10^{-3}$ fraction of floodplain area/°C/yr and $t_0 = 6.1$ years (Figures 9b and 9c). The small value of C_1 indicated that permafrost growth increased with decreasing annual temperatures. The short timescale value t_0 indicates that permafrost formation began at a rapid pace when $t = 0$ then declined by to 50% of its initial value within 6.1 years, ∼10% in 61 years, and ∼1% after 610 years. The model produced the initially rapid permafrost formation rates that we observed in the Koyukuk floodplain, with permafrost forming in ∼30%-35% of the floodplain within the first 200 years. Older deposits experienced even more rapid permafrost formation, with permafrost extending over 50%–55% of the ground within 200 years when temperatures were colder prior to 8 ka. However, permafrost extent in the model was lower in the oldest deposits compared to the

second-oldest (model results of 97% vs. 89%, respectively), similar to the measurements (86% vs. 78%), because the temperature at 9.30 ka was slightly warmer than at 8.09 ka. Our method of grouping the floodplain into discrete age classes likely produced more abrupt increases in permafrost formation rates (Figure 9c) than actually occurred. However, some spikes in floodplain-averaged permafrost formation rate should be expected when cutoffs cause large deposits to be abandoned simultaneously.

Permafrost extent increased very slowly for deposits greater than 1 Kyr old. In reality, these deposits were likely continuously experiencing local permafrost formation and degradation due to differences in snowfall, vegetation, fires, flooding, and groundwater flow, producing slow net rates that may have tended toward a dynamic equilibrium. The timing of permafrost growing from 50% to 80% of floodplain extent coincided with a significant change in floodplain hydrology, that promotes formation of a black spruce bog which gradually erases geomorphic evidence of channel migration (Figure 8).

Model results agreed with observations that permafrost has been actively forming on the floodplain through the present day—particularly since field observations revealed permafrost in recent deposits (Figure 5). The model predicted permafrost extent for each age bin within 10% of the observed value (Figure 9d). This error could be due to uncertainty in the model as well as the observed 21% inaccuracy in the permafrost map. Floodplain deposits <1 ka contained discontinuous permafrost based both on field observations and the permafrost map (Figure 7), and we observed permafrost in deposits that were decades old and wooded. Model results indicated recent climatic warming had slowed permafrost formation and mean annual air temperatures were approaching values where new permafrost would not form (i.e., where $G < 0$; Figure 9).

5. Discussion

5.1. Floodplain Permafrost Occurrence and Relationship With Vegetation Succession

Our results agree with the canonical view that vegetation succession enables rapid permafrost formation when spruce trees have grown on new bars, which typically takes 200 years for interior Alaskan rivers (e.g., Shur & Jorgenson, 2007; Viereck, 1970). We found that permafrost formation in Koyukuk floodplain deposits began soon after their deposition, with permafrost extents of ∼50% of the deposit area developing within ∼200 years. This was consistent with observations from discontinuous permafrost floodplains elsewhere in interior Alaska (e.g., Shur & Jorgenson, 2007; Viereck, 1970; Yarie et al., 1998). While we were not able to quantify decadal-to-centennial rates of permafrost formation in detail due to the floodplain deposit age fidelity, our modeling results required including this rapid initial permafrost formation via a logarithmic function to match our observations for permafrost extent and vegetation in the youngest deposits.

Focusing on permafrost formation from 200 to 10,000 years, our model predicts that rates gradually declined following sediment deposition as a logarithmic function (Figure 9). This culminates in a relatively stable permafrost extent that varies based on the range of air temperatures that the floodplain has been exposed to since it was deposited, with older floodplain deposits experiencing more rapid early permafrost formation that produced slightly greater permafrost extent in the present. During the period of rapid permafrost formation, deciduous trees with sparse permafrost are replaced by spruce with abundant permafrost, while permafrost extent within wetland and scrub/shrub vegetation increases (Figure 8). All geomorphic units experienced an increase in permafrost extent prior to 4 ka, with slightly higher permafrost extent on scroll bar ridges (typically occupied by evergreen forest) versus troughs. Koyukuk floodplain deposits with the greatest permafrost extent were >4 ka and comprised of a distinctive, undifferentiated geomorphic unit in which scroll bar sequences have been buried or reworked and vegetation consists of black spruce and herbaceous wetlands. These deposits are similar to "abandoned floodplain" terraces of the Colville River delta, which were dated to 3–4 ka using radiocarbon ages of basal peat layers (Jorgenson et al., 1998), as well as others in floodplains across interior Alaska (e.g., Mann et al., 1995). There was not a significant corresponding increase in air temperature at 4 ka (Marsicek et al., 2018), which could have altered the rate of permafrost formation (Figure 9). Therefore, we expect that processes that led to a lack of geomorphic features in undifferentiated units are slow-acting and occur to this day, such as overbank floods depositing fine sediment, sediment compaction, growth of mosses, and cryoturbation (Drury, 1956; Kanevskiy et al., 2014). These slow-acting processes produced an abrupt change in floodplain vegetation and geomorphology for deposits greater than 4 Kyr old, likely due to high permafrost extents and thick silt deposits reducing infiltration rates (e.g., Kurylyk et al., 2016) and ensuring soils remained saturated for much of the year (Viereck, 1970). Wet soils are favorable conditions for black spruce and moss growth, and developing a thick

layer of moss further insulates the ground and reduces active layer thickness (Shur & Jorgenson, 2007). Thus, the development of extensive permafrost in these older deposits appears to drive the pace of ecological succession, rather than be controlled by it.

5.2. Conceptual Model for Slow Permafrost Formation

After ~200 years, permafrost occupies around 50% of the floodplain while the remaining deposits lacks permafrost. Permafrost formation in these deposits appears to have been very slow, occurring at a rate of <10% of floodplain area per millennia (Figure 9). These slow rates of permafrost formation are puzzling as epigenetic freezing is expected to occur over years to decades, not millennia, for mean annual temperatures sufficiently below 0°C (Shur & Jorgenson, 2007). Instead, we propose that permafrost may actually be in the land pixels where the Pastick map predicts no permafrost (Figure 4), but it has little influence on above-ground vegetation due to a thick active layer.

Consider a representative lengthscale (L; m) for thermal diffusion as a function of the soil thermal conductivity (κ; J/kg/K), temperature oscillation timescale (T; s), specific heat (c_p; J/kg/K), and dry density (ρ; kg/m^3) so that $L = \sqrt{\kappa T / c_p \rho}$ (Anisimov et al., 1997; Wang et al., 2020). We used values for unfrozen, drained sand, silt, and clay from Anisimov et al. (1997) such that κ is 1.05, 1.05, and 0.90 J/kg/K; c_p is 690, 730, and 900 J/kg/K; and ρ is 1,300, 1,400, and 1,500 kg/m^3 respectively. Using T = 6 months, we found that silt and clay had characteristic lengthscales 6% and 25% less than sand, respectively. Using thermal diffusivities for dry peat and vegetation from Anisimov et al. (1997) produces lengthscales ranging from 78% less to 215% greater than that of sand. Since new point bar deposits are comprised primarily of sand and gradually develop a layer of fine-grained, organic-rich overbank deposits through repeated flood deposits, the decrease in lengthscale of thermal diffusion for silt and clay indicates that the active layer thickness should decrease for older deposits. In addition, silt and clay have higher water retention than sand, leading to a higher latent heat of fusion and making them more likely to remain frozen during subsequent summers. Therefore, we propose that permafrost might start forming in sandy point bar deposits relatively quickly, perhaps within decades. But it forms at depths where it may not substantially impact vegetation growth, promote peat formation, and be detected by permafrost probing due to active layer thicknesses that substantially exceed 1 m. Similar to the conceptual model of Shur and Jorgenson (2007), we suggest that overbank accumulation of mud over thousands of years provides an insulating layer that causes the active layer to gradually thin. As the active layer thins, permafrost eventually affects vegetation succession and becomes apparent in measurements that probe the top 1 m. Thus, the rates of overbank mud accretion, along with organic litter accumulation, might pace the rate of permafrost formation in the upper few meters of floodplain sediment.

Field observations support that permafrost extent can be driven by the thickening of fine-grained overbank deposits, linking river sediment loads and flood frequencies to groundwater connectivity and floodplain OC storage. While overbank floods can cause top-down thawing of permafrost due to transport of warm water across the landscape (Y. Zhang et al., 2023; Zheng et al., 2019), overbank deposits had some of the highest predicted permafrost extents for each deposit age on the Koyukuk floodplain (Figure 8). Therefore, while overbank floods produced short-term thawing, particularly when water ponds in scroll bar troughs, they also deposited insulating mud that ultimately led to a thinner active layer (Mann et al., 1995). Older floodplain deposits contain an upper layer of insulating peat, but the peat is underlain by thick layers of ice-rich silt that predates significant peat formation (Douglas et al., 2022). Similar deposits in the Colville (Jorgenson et al., 1998; Stephani et al., 2020), Tanana (Mann et al., 1995), and Chena (Viereck, 1970) River floodplains indicate that thick silt deposits gradually grade to peat. This implies that rivers with high sediment loads, frequent floods, and rapid aggradation rates should rapidly deposit mud on their floodplains and promote more extensive permafrost formation and peat accumulation.

5.3. Future of the Koyukuk River Floodplain

Our observations indicate that permafrost continues to form on the Koyukuk floodplain, maintaining the same pattern of rapid formation rates in young deposits and slower formation rates in older deposits (Figure 9). This trend might be complicated by further changes in air temperature decreasing formation rate (G), as well as additional climatic changes that were not considered in our simple model that promote or impede permafrost formation. For example, changes in snowfall might help to insulate the ground in the winter and impede permafrost formation (Ling & Zhang, 2003; Park et al., 2015; T. Zhang, 2005). Variations in snowfall and

redistribution of fallen snow by wind could also account for the high spatial variability in permafrost extent across all ages of floodplain deposits (Jafarov et al., 2018). Climatic warming is also causing river discharge to increase, potentially increasing flood frequency (Brabets & Walvoord, 2009; Peterson et al., 2002). More frequent floods would inhibit the establishment of white spruce forests necessary for permafrost to form in new deposits (Yarie et al., 1998), though increasing overbank deposition rates would promote permafrost growth and organic carbon storage in peat in locations where permafrost remains stable. Within these limitations, our model provides a framework for quantifying and making predictions for discontinuous permafrost formation rates driven by riverine sediment deposition and moss growth.

Both permafrost extent and overbank deposit thickness might affect rates of river migration (Figure 7). The Koyukuk River is much deeper (12.4 m) than the floodplain active layer (~0.4–2 m) but shallower than the estimated thickness of permafrost (31 m) (Jorgenson et al., 2008), so permafrost might significantly impact rates of channel migration. For instance, bank migration is expected to be limited by the rate at which ice-rich permafrost can be thawed (Costard et al., 2003; Douglas & Lamb, 2024), causing permafrost to slow channel migration (Rowland, Crosby, et al., 2023; Rowland, Schwenk, et al., 2023). Older floodplain deposits contain permafrost as well as thick overbank deposits with fine sediment and abundant moss, which can require high stresses to erode and might further slow erosion even when these deposits are partially thawed during summer months (Figure 3d; Douglas et al., 2023). While shrubification might decrease rates of riverbank erosion by increasing root cohesion (Ielpi, Lapôtre, et al., 2023), it seems unlikely that shrubification will have a major effect on the Koyukuk since the river cutbanks are already forested, the river is much deeper than typical shrub rooting depths, and a thicker active layer due to changes in snow accumulation would remain much less than the channel depth. Therefore, if the climate continues to warm and permafrost begins thawing across the Koyukuk floodplain (Figure 8), we expect that channel migration rates will increase.

Increasing river migration rates and decreasing permafrost formation rates both threaten to decrease permafrost extent in river floodplains. Since cutbank erosion and heat transfer through river banks and beds can cause permafrost thaw and mobilization tens of meters below the surface, floodplains are vulnerable to rapid thaw and abrupt release of carbon (Turetsky et al., 2020). Our model provides insight into possible future scenarios for the Koyukuk and other permafrost floodplains. For example, consider a simple estimate based on mass balance of permafrost in the floodplain:

$$\frac{d\psi_{pf}}{dt} \sim G - f_{pf} E L_r / A_{fp}, \tag{5}$$

where f_{pf} is the dimensionless fraction of cutbank length eroded that contains permafrost, E (m/yr) is the river erosion rate, L_r (m) is the downstream river length, and A_{fp} (m^2) is the total floodplain area. Equation 5 states that the areal extent of permafrost changes in time based on the imbalance between permafrost formation in new bars (G) and permafrost loss through bank erosion (E). Here we neglect top-down deepening of the active layer to better illustrate the importance of river lateral migration in dictating the fate of deep permafrost.

With a warming climate, we expect G to decrease following Equation 2 (Figure 9). In fact, the low value of G that we found on the modern Koyukuk and expect on other discontinuous permafrost floodplains indicated that small increases in air temperature may result in G approaching zero. In addition, more rapid channel migration, longer open-water seasons, and thawing permafrost would increase E (Douglas & Lamb, 2024; Gautier et al., 2021; Rowland, Crosby, et al., 2023; Rowland, Schwenk, et al., 2023). River erosion preferentially reworks younger deposits close to the modern channel, which have a low f_{pf}, but would eventually rework older deposits containing relict permafrost (high f_{pf}) far from the Koyukuk's present course (Bradley & Tucker, 2013; Ielpi, Viero, et al., 2023; Torres et al., 2017). Therefore, as shown by Equation 5, both increased bank erosion rates (E) and decreased permafrost formation rates (G) could cause rapid decline permafrost areal extent ($\frac{d\psi_{pf}}{dt} < 0$), leaving isolated permafrost to persist only in old deposits far from the modern channel.

6. Conclusions

Arctic floodplains experience continual permafrost thaw and erosion due to river migration that can be balanced by permafrost formation in new bar deposits. While physical models exist for permafrost riverbank erosion, the rate and extent of permafrost formation in newly deposited bars remains poorly quantified. Prior studies found

that vegetation succession enables permafrost formation by insulating the ground during the summer so that permafrost does not form until a white spruce forest with mossy ground cover grows. However, older floodplain deposits have been observed to contain much higher ground ice content and have a distinctive vegetation consisting of peat and black spruce bogs. The nature and timing of this transition remains enigmatic, yet it is critical to understanding the formation of permafrost- and peat-rich deposits that characterize much of Arctic floodplains, which may be destabilized during climatic warming.

This study focused on the Koyukuk River, which meanders across its floodplain. Radiocarbon and OSL dating indicate that floodplain deposits are up to 10 ka, and the spatial distribution of deposit ages illustrates how the river preferentially reworks nearby deposits with lower permafrost extents. Patterns of river migration and point bar deposition were the primary controls on permafrost presence within the floodplain, with older deposits containing more extensive permafrost and thermokarst landforms while younger deposits contained patchy permafrost. Using a calibrated permafrost map and the NLCD vegetation classifications, we examined whether vegetation drove permafrost formation or vice-versa over millennial timescales. We found that the growth of white spruce over 200 years only explains a portion (~50%) of permafrost areal extent. A later landscape change from white spruce forest to peat bog with sparse black spruce took place along the Koyukuk as deposits aged from 3.44 to 4.27 Kyr and was accompanied with more extensive permafrost formation up to 85% of the floodplain area. We attributed this change to gradual deposition of silt by overbank floods insulating the ground, leading to the formation extensive that inhibited groundwater infiltration and drove a transition in vegetation to peat, shrubs, and black spruce trees.

Model results and measurements indicated that discontinuous permafrost has been re-forming on the Koyukuk River floodplain for the last 10 Kyr. While permafrost has continued to form over the last century, our results highlight that it takes thousands of years to form permafrost-rich deposits (with >50% areal extent) that characterize ~25% of the floodplain. In recent years, warming air temperatures have likely slowed permafrost formation in the Koyukuk floodplain and increased rates of bank erosion (Rowland, Crosby, et al., 2023; Rowland, Schwenk, et al., 2023). The slow rates of permafrost formation combined with the susceptibility to bank erosion of older deposits containing extensive permafrost, excess ground ice, and carbon-rich peat would significantly decrease the carbon storage capacity and ground stability of the floodplain. Our results highlight the vulnerability of the Koyukuk floodplain to rapid landscape transformation, while our simplified model offers a framework to assess the vulnerability of other Arctic floodplains to permafrost loss.

Acknowledgments
We thank the Koyukuk-hotana Athabascans, Chief Carl Burgett, and the Huslia Tribal Council for access to their land, and USFWS—Koyukuk National Wildlife refuge for research permitting and logistical assistance. We acknowledge Alvin Attla, Darin Dayton, Shawn Huffman, Charlene Mayo, Mary Ann Sam, and Virgil Umphenour for field logistical support and local expertise. We thank Rain Blankenship, Hannah Dion-Kirshner, Kieran Dunne, Emily Geyman, John Magyar, Edda Mutter, Justin Nghiem, Jocelyn Reahl, Emily Seelen, Isabel Smith, and Lisa Winter for their assistance during fieldwork. We thank Cindy Lou Skipper and Diana Valenzuela Davila for sample preparation, as well as Alessandro Ielpi and three anonymous reviewers for their constructive feedback. Financial support was provided by the NSF Awards 2127442 and 2031532; Foster and Coco Stanback; the Linde Family; the Caltech Terrestrial Hazards Observation and Reporting (THOR) Center; the Resnick Sustainability Institute; the National Defense Science and Engineering Graduate Fellowship (MMD and PCK); the Fannie and John Hertz Foundation Cohen/Jacobs and Stein Family Fellowship (PCK); and a Department of Energy Office of Science, Biological and Environmental Research Subsurface Biogeochemical Research (SBR) Program Early Career award (JCR).

Conflict of Interest

The authors declare no conflicts of interest relevant to this study.

Data Availability Statement

Geochemical data is available in this manuscript or was previously published in Douglas et al. (2021, 2022) and is available at https://data.ess-dive.lbl.gov/datasets/doi:10.15485/1910300. Maxar imagery was previously released as part of Schwenk et al. (2023). ESRI shapefiles of geomorphic and relative age maps plus permafrost probe measurements are available at https://data.ess-dive.lbl.gov/view/doi%3A10.15485%2F2204419. Mapping was done on QGIS (https://www.qgis.org/en/site/) using the version 3.4.13 long-term release and analyses were done in Matlab v2021 under academic license to Caltech.

References

Alley, R. B. (2004). *GISP2 ice core temperature and accumulation data* (Vol. 13, p. 2004). IGBP PAGES/World Data Center for Paleoclimatology Data Contribution Series.

Anisimov, O. A., Shiklomanov, N. I., & Nelson, F. E. (1997). Global warming and active-layer thickness: Results from transient general circulation models. *Global and Planetary Change*, *15*(3), 61–77. https://doi.org/10.1016/S0921-8181(97)00009-X

Biskaborn, B. K., Smith, S. L., Noetzli, J., Matthes, H., Vieira, G., Streletskiy, D. A., et al. (2019). Permafrost is warming at a global scale. *Nature Communications*, *10*(1), 1–11. https://doi.org/10.1038/s41467-018-08240-4

Brabets, T. P., & Walvoord, M. A. (2009). Trends in streamflow in the Yukon River Basin from 1944 to 2005 and the influence of the Pacific Decadal Oscillation. *Journal of Hydrology*, *371*(1), 108–119. https://doi.org/10.1016/j.jhydrol.2009.03.018

Brabets, T. P., Wang, B., & Meade, R. H. (2000). *Environmental and hydrologic overview of the Yukon River Basin, Alaska and Canada* (Vol. 99). US Department of the Interior, US Geological Survey. Retrieved from https://pubs.usgs.gov/wri/wri994204/

Bradley, D. N., & Tucker, G. E. (2013). The storage time, age, and erosion hazard of laterally accreted sediment on the floodplain of a simulated meandering river. *Journal of Geophysical Research: Earth Surface*, *118*(3), 1308–1319. https://doi.org/10.1002/jgrf.20083

Chadburn, S. E., Burke, E. J., Cox, P. M., Friedlingstein, P., Hugelius, G., & Westermann, S. (2017). An observation-based constraint on permafrost loss as a function of global warming. *Nature Climate Change*, *7*(5), 340–344. https://doi.org/10.1038/nclimate3262

Costard, F., Dupeyrat, L., Gautier, E., & Carey-Gailhardis, E. (2003). Fluvial thermal erosion investigations along a rapidly eroding river bank: Application to the Lena River (central Siberia). *Earth Surface Processes and Landforms*, *28*(12), 1349–1359. https://doi.org/10.1002/esp.592

Crampton, C. B. (1979). Changes in permafrost distribution produced by a migrating river meander in the northern Yukon, Canada. *Arctic*, *32*(2), 148–151. https://doi.org/10.14430/arctic2613

Daly, C., Smith, J., & Halbleib, M. (2018). 1981-2010 high-resolution temperature and precipitation maps for Alaska final report (Vol. *43*).

Delisle, G. (1998). Numerical simulation of permafrost growth and decay. *Journal of Quaternary Science*, *13*(4), 325–333. https://doi.org/10.1002/(SICI)1099-1417(199807/08)13:4<325::AID-JQS385>3.0.CO;2-A

del Valle, J. I., Guarín, J. R., & Sierra, C. A. (2014). Unambiguous and low-cost determination of growth rates and ages of tropical trees and palms. *Radiocarbon*, *56*(1), 39–52. https://doi.org/10.2458/56.16486

Douglas, M. M., Dunne, K. B. J., & Lamb, M. P. (2023). Sediment entrainment and slump blocks limit permafrost riverbank erosion. *Geophysical Research Letters*, *50*(11), e2023GL102974. https://doi.org/10.1029/2023GL102974

Douglas, M. M., & Lamb, M. P. (2024). A model for thaw and erosion of permafrost riverbanks. *Journal of Geophysical Research: Earth Surface*, *129*(4), e2023JF007452. https://doi.org/10.1029/2023JF007452

Douglas, M. M., Li, G. K., Fischer, W. W., Rowland, J. C., Kemeny, P. C., West, A. J., et al. (2022). Organic carbon burial by river meandering partially offsets bank erosion carbon fluxes in a discontinuous permafrost floodplain. *Earth Surface Dynamics*, *10*(3), 421–435. https://doi.org/10.5194/esurf-10-421-2022

Douglas, M. M., Lingappa, U. F., Lamb, M. P., Rowland, J. C., West, A. J., Li, G., et al. (2021). Impact of river channel lateral migration on microbial communities across a discontinuous permafrost floodplain. *Applied and Environmental Microbiology*, *87*(20), e01339-21. https://doi.org/10.1128/AEM.01339-21

Drury, W. H. (1956). Bog flats and physiographic processes in the Upper Kuskokwim River Region, Alaska. *Contributions from the Gray Herbarium of Harvard University*, *178*, 1–130. https://doi.org/10.5962/p.336377

England, M. R., Eisenman, I., Lutsko, N. J., & Wagner, T. J. W. (2021). The recent emergence of Arctic amplification. *Geophysical Research Letters*, *48*(15), e2021GL094086. https://doi.org/10.1029/2021GL094086

Farquharson, L., Bodony, K., Mann, D., & Jones, B. (2011). Nogahabara reconnaissance and initial findings, notes from the August 2011 field trip.

French, H., & Shur, Y. (2010). The principles of cryostratigraphy. *Earth-Science Reviews*, *101*(3), 190–206. https://doi.org/10.1016/j.earscirev.2010.04.002

Gautier, E., Dépret, T., Cavero, J., Costard, F., Virmoux, C., Fedorov, A., et al. (2021). Fifty-year dynamics of the Lena River islands (Russia): Spatio-temporal pattern of large periglacial anabranching river and influence of climate change. *Science of the Total Environment*, *783*, 147020. https://doi.org/10.1016/j.scitotenv.2021.147020

Gill, D. (1975). Influence of white spruce trees on permafrost-table microtopography, Mackenzie River Delta. *Canadian Journal of Earth Sciences*, *12*(2), 263–272. https://doi.org/10.1139/e75-023

Ielpi, A., Lapôtre, M. G. A., Finotello, A., & Roy-Léveillée, P. (2023). Large sinuous rivers are slowing down in a warming Arctic. *Nature Climate Change*, *13*(4), 1–7. https://doi.org/10.1038/s41558-023-01620-9

Ielpi, A., Viero, D. P., Lapôtre, M. G. A., Graham, A., Ghinassi, M., & Finotello, A. (2023). How is time distributed in a river meander belt? *Geophysical Research Letters*, *50*(2), e2022GL101285. https://doi.org/10.1029/2022GL101285

Isaksen, K., Romanovsky, V., Smith, S. L., & Drozdov, D. S. (2016). Thermal state of permafrost across the circumpolar permafrost regions–results from the latest assessment report, the SWIPA update. In F. Günther, & A. Morgenstern (Eds.), *XI international conference on permafrost, book of abstracts* (pp. 444–445). Bibliothek Wissenschaftspark Albert Einstein.

Jafarov, E. E., Coon, E. T., Harp, D. R., Wilson, C. J., Painter, S. L., Atchley, A. L., & Romanovsky, V. E. (2018). Modeling the role of preferential snow accumulation in through talik development and hillslope groundwater flow in a transitional permafrost landscape. *Environmental Research Letters*, *13*(10), 105006. https://doi.org/10.1088/1748-9326/aadd30

Jorgenson, M. T., Shur, Y. L., & Walker, H. J. (1998). Evolution of a permafrost-dominated landscape on the Colville River Delta, northern Alaska. In *Proceedings of the 7th international conference on permafrost* (Vol. 55, pp. 523–529). Yellowknife. Collection Nordicana.

Jorgenson, M. T., Yoshikawa, K., Kanevskiy, M., Shur, Y., Romanovsky, V., Marchenko, S., et al. (2008). *Permafrost characteristics of Alaska*. University of Alaska.

Kanevskiy, M., Jorgenson, T., Shur, Y., O'Donnell, J. A., Harden, J. W., Zhuang, Q., & Fortier, D. (2014). Cryostratigraphy and permafrost evolution in the Lacustrine lowlands of West-Central Alaska. *Permafrost and Periglacial Processes*, *25*(1), 14–34. https://doi.org/10.1002/ppp.1800

Kanevskiy, M., Shur, Y., Strauss, J., Jorgenson, T., Fortier, D., Stephani, E., & Vasiliev, A. (2016). Patterns and rates of riverbank erosion involving ice-rich permafrost (yedoma) in northern Alaska. *Geomorphology*, *253*, 370–384. https://doi.org/10.1016/j.geomorph.2015.10.023

Karjalainen, O., Aalto, J., Luoto, M., Westermann, S., Romanovsky, V. E., Nelson, F. E., et al. (2019). Circumpolar permafrost maps and geohazard indices for near-future infrastructure risk assessments. *Scientific Data*, *6*(1), 1–16. https://doi.org/10.1038/sdata.2019.37

Kaufman, D. S., Axford, Y. L., Henderson, A. C. G., McKay, N. P., Oswald, W. W., Saenger, C., et al. (2016). Holocene climate changes in eastern Beringia (NW North America)—A systematic review of multi-proxy evidence. *Quaternary Science Reviews*, *147*, 312–339. https://doi.org/10.1016/j.quascirev.2015.10.021

Kreig, R. A., & Reger, R. D. (1982). *Air-photo analysis and summary of landform soil properties along the route of the Trans-Alaska Pipeline System*. Division of Geological & Geophysical Surveys.

Kurylyk, B. L., Hayashi, M., Quinton, W. L., McKenzie, J. M., & Voss, C. I. (2016). Influence of vertical and lateral heat transfer on permafrost thaw, peatland landscape transition, and groundwater flow. *Water Resources Research*, *52*(2), 1286–1305. https://doi.org/10.1002/2015WR018057

Lauer, J. W., & Parker, G. (2008). Net local removal of floodplain sediment by river meander migration. *Geomorphology*, *96*(1), 123–149. https://doi.org/10.1016/j.geomorph.2007.08.003

Lauer, J. W., & Willenbring, J. (2010). Steady state reach-scale theory for radioactive tracer concentration in a simple channel/floodplain system. *Journal of Geophysical Research*, *115*(F4), F04018. https://doi.org/10.1029/2009JF001480

Laxton, S., & Coates, J. (2010). Geophysical and borehole investigations of permafrost conditions associated with compromised infrastructure in Dawson and Ross River, Yukon (Vol. *14*).

Leopold, L. B., & Wolman, M. G. (1957). *River channel patterns: Braided, meandering, and straight (USGS Numbered Series No. 282- B). River channel patterns: Braided, meandering, and straight* (Vol. 282-B, p. 50). U.S. Government Printing Office. https://doi.org/10.3133/pp282B

Ling, F., & Zhang, T. (2003). Impact of the timing and duration of seasonal snow cover on the active layer and permafrost in the Alaskan Arctic. *Permafrost and Periglacial Processes*, *14*(2), 141–150. https://doi.org/10.1002/ppp.445

Mann, D. H., Fastie, C. L., Rowland, E. L., & Bigelow, N. H. (1995). Spruce succession, disturbance, and geomorphology on the Tanana River floodplain, Alaska. *Écoscience*, *2*(2), 184–199. https://doi.org/10.1080/11956860.1995.11682283

Marsicek, J., Shuman, B. N., Bartlein, P. J., Shafer, S. L., & Brewer, S. (2018). Reconciling divergent trends and millennial variations in Holocene temperatures. *Nature*, *554*(7690), 92–96. https://doi.org/10.1038/nature25464

Meyer, H., Schirrmeister, L., Yoshikawa, K., Opel, T., Wetterich, S., Hubberten, H.-W., & Brown, J. (2010). Permafrost evidence for severe winter cooling during the Younger Dryas in northern Alaska. *Geophysical Research Letters*, *37*(3), L03501. https://doi.org/10.1029/2009GL041013

Miall, A. D. (2006). *The geology of fluvial deposits*. Springer Berlin Heidelberg. https://doi.org/10.1007/978-3-662-03237-4

Minsley, B. J., Abraham, J. D., Smith, B. D., Cannia, J. C., Voss, C. I., Jorgenson, M. T., et al. (2012). Airborne electromagnetic imaging of discontinuous permafrost. *Geophysical Research Letters*, *39*(2), L02503. https://doi.org/10.1029/2011GL050079

Nowacki, G. J., Spencer, P., Fleming, M., Brock, T., & Jorgenson, T. (2003). *Unified ecoregions of Alaska: 2001 (USGS numbered series No. 2002–297)*. Geological Survey. Retrieved from http://pubs.er.usgs.gov/publication/ofr2002297

Obu, J., Westermann, S., Bartsch, A., Berdnikov, N., Christiansen, H. H., Dashtseren, A., et al. (2019). Northern Hemisphere permafrost map based on TTOP modelling for 2000–2016 at 1 km^2 scale. *Earth-Science Reviews*, *193*, 299–316. https://doi.org/10.1016/j.earscirev.2019.04.023

Park, H., Fedorov, A. N., Zheleznyak, M. N., Konstantinov, P. Y., & Walsh, J. E. (2015). Effect of snow cover on pan-Arctic permafrost thermal regimes. *Climate Dynamics*, *44*(9), 2873–2895. https://doi.org/10.1007/s00382-014-2356-5

Parker, G., Shimizu, Y., Wilkerson, G. V., Eke, E. C., Abad, J. D., Lauer, J. W., et al. (2011). A new framework for modeling the migration of meandering rivers. *Earth Surface Processes and Landforms*, *36*(1), 70–86. https://doi.org/10.1002/esp.2113

Pastick, N. J., Jorgenson, M. T., Wylie, B. K., Nield, S. J., Johnson, K. D., & Finley, A. O. (2015). Distribution of near-surface permafrost in Alaska: Estimates of present and future conditions. *Remote Sensing of Environment*, *168*, 301–315. https://doi.org/10.1016/j.rse.2015.07.019

Pekel, J.-F., Cottam, A., Gorelick, N., & Belward, A. S. (2016). High-resolution mapping of global surface water and its long-term changes. *Nature*, *540*(7633), 418–422. https://doi.org/10.1038/nature20584

Peterson, B. J., Holmes, R. M., McClelland, J. W., Vörösmarty, C. J., Lammers, R. B., Shiklomanov, A. I., et al. (2002). Increasing river discharge to the Arctic Ocean. *Science*, *298*(5601), 2171–2173. https://doi.org/10.1126/science.1077445

Reimer, P. J., Austin, W. E. N., Bard, E., Bayliss, A., Blackwell, P. G., Ramsey, C. B., et al. (2020). The IntCal20 northern hemisphere radiocarbon age calibration curve (0–55 cal kBP). *Radiocarbon*, *62*(4), 725–757. https://doi.org/10.1017/RDC.2020.41

Reimer, P. J., Brown, T. A., & Reimer, R. W. (2004). Discussion: Reporting and calibration of post-bomb ^{14}C data. *Radiocarbon*, *46*(3), 1299–1304. https://doi.org/10.1017/S0033822200033154

Reimer, R. W., & Reimer, P. J. (2023). CALIBomb. Retrieved from https://calib.org/CALIBomb/

Roux, N., Costard, F., & Grenier, C. (2017). Laboratory and numerical simulation of the evolution of a river's talik. *Permafrost and Periglacial Processes*, *28*(2), 460–469. https://doi.org/10.1002/ppp.1929

Rowland, J. C., Crosby, B., Schwenk, J., Piliouras, A., & Douglas, M. (2023). Riverbank temperatures on the Selawik River, Alaska 2010-2012, and Koyukuk River, Alaska June to July 2018. *Environmental System Science Data Infrastructure for a Virtual Ecosystem (ESS-DIVE) (United States); Incorporating the Hydrological Controls on Carbon Cycling in Floodplain Ecosystems into Earth System Models (ESMs)*. https://doi.org/10.15485/1922885

Rowland, J. C., Schwenk, J. P., Shelef, E., Muss, J., Ahrens, D., Stauffer, S., et al. (2023). Scale-dependent influence of permafrost on riverbank erosion rates. *Journal of Geophysical Research: Earth Surface*, *128*(7), e2023JF007101. https://doi.org/10.1029/2023JF007101

Rowland, J. C., Shelef, E., Pope, P. A., Muss, J., Gangodagamage, C., Brumby, S. P., & Wilson, C. J. (2016). A morphology independent methodology for quantifying planview river change and characteristics from remotely sensed imagery. *Remote Sensing of Environment*, *184*, 212–228. https://doi.org/10.1016/j.rse.2016.07.005

Rowland, J. C., & Stauffer, S. (2019). Classified channel masks of portions of 13 rivers across the Arctic and areas of floodplain erosion and accretion ranging from 1973 to 2016. https://doi.org/10.15485/1571525

Schwab, M. S., Hilton, R. G., Raymond, P. A., Haghipour, N., Amos, E., Tank, S. E., et al. (2020). An abrupt aging of dissolved organic carbon in large Arctic rivers. *Geophysical Research Letters*, *47*(23), e2020GL088823. https://doi.org/10.1029/2020GL088823

Schwenk, J., Piliouras, A., & Rowland, J. (2023). Observations and machine-learned models of near-surface permafrost along the Koyukuk River, Alaska, USA. *Environmental System Science Data Infrastructure for a Virtual Ecosystem (ESS-DIVE) (United States)*. https://doi.org/10.15485/1922517

Shur, Y. L., & Jorgenson, M. T. (2007). Patterns of permafrost formation and degradation in relation to climate and ecosystems. *Permafrost and Periglacial Processes*, *18*(1), 7–19. https://doi.org/10.1002/ppp.582

Smith, S. L., O'Neill, H. B., Isaksen, K., Noetzli, J., & Romanovsky, V. E. (2022). The changing thermal state of permafrost. *Nature Reviews Earth & Environment*, *3*(1), 10–23. https://doi.org/10.1038/s43017-021-00240-1

Stephani, E., Drage, J., Miller, D., Jones, B. M., & Kanevskiy, M. (2020). Taliks, cryopegs, and permafrost dynamics related to channel migration, Colville River Delta, Alaska. *Permafrost and Periglacial Processes*, *31*(2), 239–254. https://doi.org/10.1002/ppp.2046

Torres, M. A., Limaye, A. B., Ganti, V., Lamb, M. P., West, A. J., & Fischer, W. W. (2017). Model predictions of long-lived storage of organic carbon in river deposits. *Earth Surface Dynamics*, *5*(4), 711–730. https://doi.org/10.5194/esurf-5-711-2017

Turetsky, M. R., Abbott, B. W., Jones, M. C., Anthony, K. W., Olefeldt, D., Schuur, E. A., et al. (2020). Carbon release through abrupt permafrost thaw. *Nature Geoscience*, *13*(2), 138–143. https://doi.org/10.1038/s41561-019-0526-0

van Everdingen, R. O. (2005). *Multi-language glossary of permafrost and related ground-ice terms*. International Permafrost Association.

Viereck, L. A. (1970). Forest succession and soil development adjacent to the Chena River in Interior Alaska. *Arctic and Alpine Research*, *2*(1), 1–26. https://doi.org/10.1080/00040851.1970.12003558

Wang, K., Jafarov, E., & Overeem, I. (2020). Sensitivity evaluation of the Kudryavtsev permafrost model. *Science of the Total Environment*, *720*, 137538. https://doi.org/10.1016/j.scitotenv.2020.137538

White, K. D., & Eames, H. J. (1999). *CRREL ice jam database. (No. CRREL-99-2)*. Cold Regions Research and Engineering Lab Hanover, NH. Retrieved from https://apps.dtic.mil/docs/citations/ADA362147

Wickham, J., Stehman, S. V., Sorenson, D. G., Gass, L., & Dewitz, J. A. (2021). Thematic accuracy assessment of the NLCD 2016 land cover for the conterminous United States. *Remote Sensing of Environment*, *257*, 112357. https://doi.org/10.1016/j.rse.2021.112357

Wild, B., Andersson, A., Bröder, L., Vonk, J., Hugelius, G., McClelland, J. W., et al. (2019). Rivers across the Siberian Arctic unearth the patterns of carbon release from thawing permafrost. *Proceedings of the National Academy of Sciences of the United States of America*, *116*(21), 10280–10285. https://doi.org/10.1073/pnas.1811797116

Yarie, J., Viereck, L., Van Cleve, K., & Adams, P. (1998). Flooding and ecosystem dynamics along the Tanana River: Applying the state-factor approach to studies of ecosystem structure and function on the Tanana River floodplain. *BioScience*, *48*(9), 690–695. https://doi.org/10.2307/1313332

Zhang, T. (2005). Influence of the seasonal snow cover on the ground thermal regime: An overview. *Reviews of Geophysics*, *43*(4), RG4002. https://doi.org/10.1029/2004RG000157

Zhang, Y., Jafarov, E., Piliouras, A., Jones, B., Rowland, J. C., & Moulton, J. D. (2023). The thermal response of permafrost to coastal floodplain flooding. *Environmental Research Letters*, *18*(3), 035004. https://doi.org/10.1088/1748-9326/acba32

Zheng, L., Overeem, I., Wang, K., & Clow, G. D. (2019). Changing Arctic river dynamics cause localized permafrost thaw. *Journal of Geophysical Research: Earth Surface*, *124*(9), 2324–2344. https://doi.org/10.1029/2019JF005060